AN ABSTRACT OF THE THESIS OF

David A. Edmondson for the degree of Master of Science in Radiation Health Physics presented on June 26, 2014.

Title: Blood-Based Gene Expression as a Biodosimetry Model for Neuroblastoma Patients Treated with ^{131}I-mIBG

Abstract approved:

_____

Kathryn A. Higley

Internal dosimetry is challenging and relies on estimates using MIRD or ICRP biokinetic models. To address this, we looked at gene expression analysis in whole blood from radiotherapy patients. Patients with relapsed or refractory neuroblastoma who received ^{131}I-mIBG at UCSF were used to correlate internal ionizing radiation (IR) dose with selected gene expression. 40 patients, median age 7 years, had blood drawn at baseline, 72, 96, and 120 hours after ^{131}I-mIBG infusion. A total of 14 patients received mIBG treatment only, while 19 patients received Irinotecan and 7 received Vorinostat in combination with mIBG.

Whole body absorbed dose was calculated for each patient based on the mIBG treatment doses using MIRD internal dosimetry models. Two models were used and compared with the decision being to use a model that was predictive based on an average of three patient's responses. We then assessed transcripts using RT-PCR that were the most significant for describing the mixed therapeutic treatments over time. Modulation was evaluated statistically using multiple regression analysis for data at hours 0, 72, 96. A total of 6 genes were analyzed across 40 patients: CDKN1A,

FDXR, GADD45A, BCLXL, STAT5B, and BAX. Four genes were significantly modulated upon exposure to ^{131}I-mIBG at 72 hours, as well as at 96 hours, when controlling for dose and chemotherapy. Five genes showed significant responses to Irinotecan combined with mIBG and 2 had significant responses to Vorinostat combined with mIBG, all when controlling for time and dose. A model was then developed to predict absorbed dose based on modulation of gene transcripts within white blood cells.

This study represents a unique effort of using radiotherapy patients to characterize biomarkers that may be useful for biodosimetry and treatment. Our data indicates that transcripts, which have been previously identified as biomarkers of external exposures in *ex vivo* whole blood and *in vivo* radiotherapy patients, are also good indicators of internal exposure over time. The characterization of internal irradiation-responsive genes will provide valuable understanding of the genetic mechanisms related to internal exposures.

Blood-Based Gene Expression as a Biodosimetry Model for Neuroblastoma Patients Treated with ^{131}I-mIBG

by
David A. Edmondson

A THESIS

submitted to

Oregon State University

in partial fulfillment of
the requirements for the
degree of

Master of Science

Presented June 26, 2014
Commencement June 2015

Master of Science thesis of David A. Edmondson presented on June 26, 2014

APPROVED:

Major Professor, representing Radiation Health Physics

Head of the Department of Nuclear Engineering and Radiation Health Physics

Dean of the Graduate School

I understand that my thesis will become part of the permanent collection of Oregon State University libraries. My signature below authorizes release of my thesis to any reader upon request.

David A. Edmondson, Author

ACKNOWLEDGEMENTS

This thesis is dedicated to my grandmother who passed away during its making.

Foremost, I would like to express my sincere gratitude to my research advisor Dr. Matthew Coleman at Lawrence Livermore National Laboratory for the continuous support of my thesis study and research, for his patience, motivation, enthusiasm, and immense knowledge. His guidance helped me in all the time of research and writing of this thesis. I could not have imagined having a better advisor and mentor for my master's thesis.

I have the utmost appreciation for Dr. Steven DuBois and Dr. Erin Karski of the University of California San Francisco Children's Hospital Pediatrics Oncology division for their cooperation and support. Their help and feedback was extremely useful for the purposes of this thesis and I am very grateful for them allowing me to do my thesis as a part of their neuroblastoma study.

None of this could have happened without the support from Dr. Kathryn Higley and the entire eCampus faculty at Oregon State University. The program provided a unique opportunity with the Radiation Health Physics program for which I am extremely grateful.

Thank you to my family for always believing in me and providing me a home that gave me the opportunities I have today. Finally, to my wonderful wife, Katherine, thank you for your patience with me during my long stints of time being devoted to this product and away from you.

TABLE OF CONTENTS

TABLE OF CONTENTS (Continued)

Page

TABLE OF CONTENTS (Continued)

Page

LIST OF FIGURES

Figure Page

LIST OF TABLES

Table Page

List of Abbreviations

BER	Base Excision Repair
Bq	Becquerel
CEDE	Committed Effective Dose Equivalent
cDNA	Complementary DNA
Ct	Cycle Threshold
DNA	Deoxyribonucleic Acid
DSB	Double Strand Break
Gy	Gray
HR	Homologous Repair
ICRP	International Committee on Radiation Protection
IMRT	Intensity-Modulated Radiation Therapy
IR	Ionizing Radiation
keV	Kilo electron volt
LLNL	Lawrence Livermore National Laboratory
mIBG	Metaiodobenzylguanidine
MIRD	Medical Internal Radiation Dose
mRNA	Messenger RNA
NANT	New Approaches to Neuroblastoma Therapy
NHEJ	Non-Homologous End Joining
PCR	Polymerase Chain Reaction
RNA	Ribonucleic Acid
RT-PCR	Real-Time Polymerase Chain Reaction
REM	Radiation Equivalent Man
ROS	Reactive Oxygen Species
SSB	Single Strand Break
Sv	Sievert
TaRT	Targeted Radionuclide Therapy
TEDE	Total Effective Dose Equivalent
UCSF	University of California San Francisco

1.0 INTRODUCTION

1.1 Neuroblastoma

Neuroblastoma is the most common extracranial solid tumor in childhood accounting for about 7% of all patients younger than 15 years. This small percentage accounts for 15% of all pediatric cancer deaths (Maris, Hogarty, Bagatell, & Cohn, 2007). The tumors appear in tissue associated with the sympathetic nervous system, with 65% of the tumors developing in the abdomen and half of these from the adrenal medulla (Maris et al., 2007). In 1991, the disease occurred 1 in every 10,000 and only 30% of all diagnosed survived for greater than 5 years. The survival rate was strongly correlated with the stage of the disease when found (Fielding & Flower, 1991). And only 20% of all patients with metastatic neuroblastoma survive longer than 5 years (Matthay et al., 1998). While treatment has advanced, this statistic has barely changed.

The outcome of patients diagnosed with neuroblastoma depends upon a few factors. One is the age of diagnosis. For patients older than 18 months, the outcome is significantly less optimistic compared to earlier onset (DuBois & Matthay, 2008). Younger patients have better outlooks because they are less likely to develop recurrent disease as compared to older patients. The next factor is the presence of a mutated and amplified avian myelocytomatosis viral oncogene neuroblastoma derived homolog (MYCN). This amplified gene, a proto-oncogene, is found in approximately 20% of all tumors and is correlated with a poor outcome for patients (Maris et al., 2007). The last factor is the type of cancer found. There are three ways neuroblastoma can present itself: localized tumors, metastasis (multiple sites within the body), and

the so-called 4S, which is the most progressive form of neuroblastoma according to its anatomical presence at diagnosis (see Appendix A). A total of 40% of all cases will be with localized tumors while about half will be as metastasis with the remainder being 4S (Maris et al., 2007). Metastasis is accompanied by a poor outcome. A description of the different groups of neuroblastoma patients can be found in Appendix A.

1.2 Methods of Treatment for Neuroblastoma

Therapy differs based on the risk-group assigned to the patient. Patients with low-risk neuroblastoma are often treated with only surgery, while intermediate-risk often incorporates surgery with 4 to 8 months of multi-agent chemotherapy. High-risk patients receive intensive chemotherapy, surgery, myeloablative consolidation therapy, and targeted therapy for the small cancer left (Wolden, 2007). The more progressed and high-risk the disease, the more complex the therapy will be.

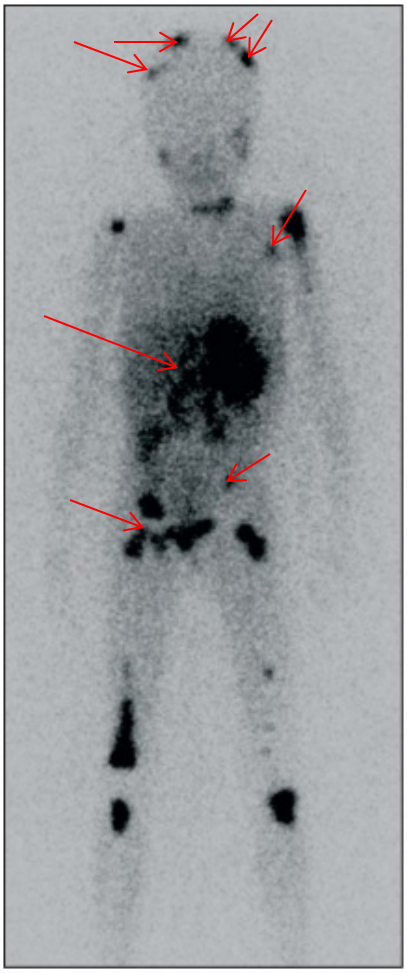

Figure 1-1 Image of Neuroblastoma Patient undergoing mIBG radiotherapy
(Figure is adapted from Maris et al., 2007) The image shows an scan of a patient after receiving mIBG treatment. Arrows indicate examples of metastatic neuroblastoma tumors.

1.2.1 Radiation Therapy

One of the primary rules of radiosensitivity of cells is that the more proliferative the cell is the more radiosensitive it is (Hall & Giaccia, 2012). This is largely because the task of undergoing mitosis requires the cell to undergo many checks and if any do not pass, the cell will die. Radiation therapy is used to take advantage of this weakness, as cancer cells are very proliferative compared to normal body cells. For this reason, radiation therapy remains one of the most prevalent and

effective forms of cancer therapy. However, even though cancer cells are more susceptible to death from radiation, normal cells are still affected. Heavy amounts of radiation induce some early effects and late effects on normal tissues, such as secondary cancers (Hall & Giaccia, 2012). In order to limit this risk, there is a strong desire to maximize the therapeutic ratio.

Two emerging strategies have the potential to achieve better therapeutic ratios, which are broadly applicable to many cancers. The first selectively directs radiation to tumor cells, most commonly by linking a therapeutic radionuclide with a targeting small molecule or monoclonal antibody. The second strategy combines radiation with drugs that preferentially sensitize tumor cells to the effects of radiation, ideally without increasing the risk of radiation injury to normal tissues. For stage III and IV neuroblastoma, both are used.

1.2.1.1 Targeted Therapy

Using radionuclide-tagged chemicals is known as targeted radionuclide therapy (TaRT). Rather than whole body radiation treatment, IMRT, or even Proton therapy, TaRT allows clinicians to target tumors directly throughout the body while sparing surrounding tissues. TaRT involves utilizing molecules that target specific tumors based upon the affinity of the tumor for that chemical. So, rather than attacking a tumor at the volume level, TaRT affects the tumor at the cellular level (Meredith, Wong, & Knox, 2007).

1.2.1.2 ^{131}I-Metaiodobenzylguanidine

Patients with advanced neuroblastoma have poor outcomes that necessitate novel treatment approaches. For patients with stage III or IV neuroblastoma, TaRT is often used and this therapy of choice uses Iodine-131 tagged metaiodobenzylguanidine (^{131}I-mIBG). ^{131}I-mIBG is a radiopharmaceutical that provides a tumor cell targeted treatment for patients with advanced neuroblastoma. MIBG, also known as Iobenguane, is a norepinephrine analogue that is quickly taken up by cells with an activated norepinephrine transporter gene (DuBois & Matthay, 2013; Vöö, Bucerius, & Mottaghy, 2011). It has been found that mIBG is stored in cytoplasm and mitochondria, rather than the neurosecretory granules that store norepinephrine (Vöö et al., 2011). 90% of all neuroblastoma tumors are mIBG-avid (DuBois & Matthay, 2008; Vöö et al., 2011).

When using mIBG as part of TaRT, the mIBG is rapidly taken up by neuroblastoma tumors with a peak at 6 hours (Vöö et al., 2011). This rapid clearing from the blood causes only 10% to remain in the blood stream within a few hours after injection (Vöö et al., 2011). According to ICRP 53, mIBG concentrates in the liver (33%), lungs (3%), heart (0.8%), spleen (0.6%), and salivary glands (0.4%), along with the tumors (ICRP, 1988). It has also been shown that approximately 15% of total injected activity immediately exits the body into the bladder (Koral et al., 2008; Matthay et al., 1998, 2001).

mIBG can be tagged with Iodine-123, Iodine-125 or Iodine 131. Each of these isotopes of Iodine has a different radioactive property that causes it to be used for a

different application. I-123 is widely used for imaging because it provides good image quality and count statistics (Monsieurs 2002). It decays by electron capture and emits a 159 keV gamma. I-125 also decays by electron capture with a 59 day half-life and emits a 35 keV gamma. I-131 decays by beta minus decay with an 8.02 day half-life and emits both a 192 keV beta particle (90%) and a 365 keV gamma (82%). I-131 was chosen over I-125 due to the range of its beta. I-125 was ineffective against larger tumor spheroids while I-131 performed well for tumors 400um or wider (DuBois & Matthay, 2008).

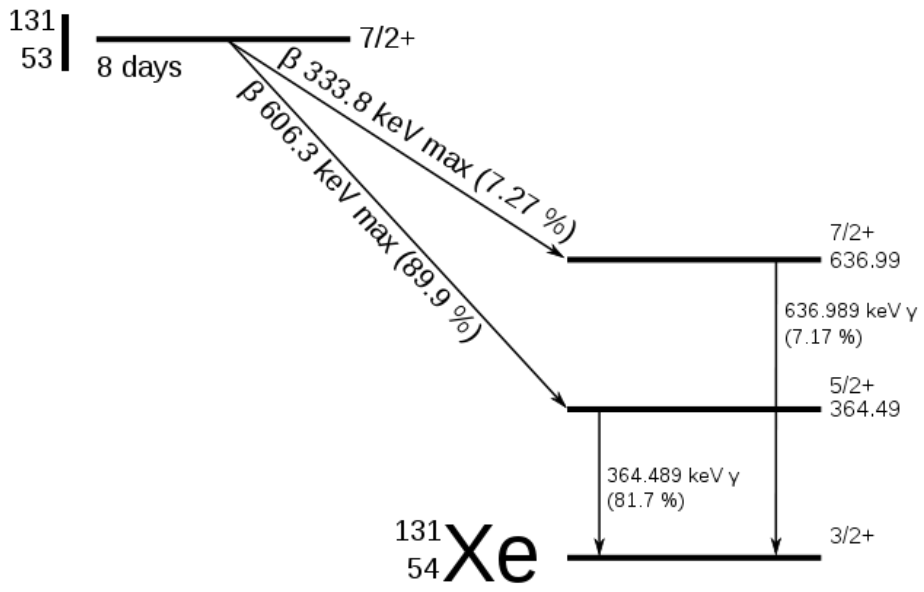

Figure 1-2 Iodine-131 Decay Tree
(http://en.wikipedia.org/wiki/File:Iodine-131-decay-scheme-simplified.svg).The image shows the decay tree for I-131 and the maximum beta energies associated.

1.2.2 Chemotherapy

Irinotecan, a camptothecin topoisomerase-1 inhibitor, and vorinostat, a histone deacetylase inhibitor, sensitize a range of cancer cells to radiation, though with

different proposed mechanisms of radiation sensitization. Camptothecins, such as irinotecan, sensitize a range of tumor cells to the effects of radiation (Chabot, 1997; Kushner, Kramer, & Modak, 2011; Vassal et al., 2008). For example, using a topoisomerase 1 inhibitor together with ^{131}I-mIBG resulted in increased cytotoxicity in neuroblastoma preclinical models (DuBois & Matthay, 2008). Radiation sensitization is directly dependent upon interaction of the camptothecin with topoisomerase-1 and does not require transcription or new protein synthesis. Radiation sensitization by camptothecins is time-dependent, with sensitization not observed when camptothecin exposure begins following radiation therapy (Chabot, 1997; Kushner et al., 2011; Vassal et al., 2008).

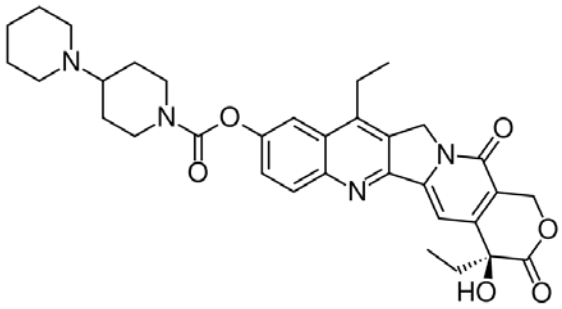

Figure 1-3 Irinotecan (http://commons.wikimedia.org/wiki/File:Irinotecan.svg)

The image shows the chemical structure of the Irinotecan.

Vorinostat and other histone deacetylase inhibitors as a class sensitize a range of tumor cells to the effects of radiation. Rather than an immediate increase in double-strand DNA breaks, histone deacetylase inhibitors prolong the presence of double-strand DNA breaks, as assessed by prolonged increases in γ-H2AX foci. This finding suggests impairment of DNA repair mechanisms and several groups have observed decreased expression of critical DNA repair proteins (Rad51, Rad52, Ku70,

Ku80, and Ku86) after histone deacetylase inhibitor therapy (DuBois & Matthay, 2013; Fantin, Loboda, & Paweletz, 2008; More, Itsara, Yang, & Geier, 2011; Munshi et al., 2006; Richon, 2006).

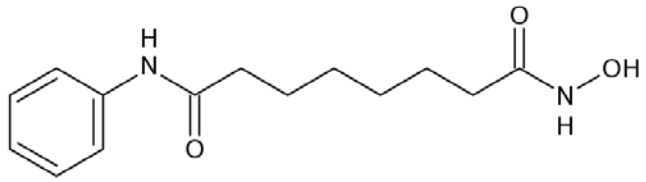

Figure 1-4 Vorinostat (http://commons.wikimedia.org/wiki/File:Vorinostat.svg)

The image shows the chemical composition of the Vorinostat pharmaceutical.

1.3 Biological Effects of Radiation

Independent of the IR source, DNA constitutes the most critical target of IR (Hall & Giaccia, 2012). There are two types of damage that can occur to the DNA, direct and indirect damage. DNA lesion encompass DNA single and double strand breaks (SSB and DSBs, respectively), DNA base damage and apyrimidinic/apurinic sites as well as DNA-protein crosslinks. Although DSBs may be the most deleterious of DNA damages caused by IR and the most relevant lesions to trigger a cellular ionizing radiation response (Hall & Giaccia, 2012), other DNA lesions may also have carcinogenic consequences. There is also evidence that damage to mitochondria might be a significant trigger for radiation response in cells (Budworth et al., 2012; Knops, Boldt, Wolkenhauer, & Kriehuber, 2012; S Paul & Amundson, 2008).

Alternatively, IR may interact with other atoms or molecules in the cell, producing free radicals such as reactive oxygen species (ROSs), which are generated by the ionization of water and iron related Fenton reactions within the cells. Radiolysis of water does not occur via Equation 1.1 because only one molecule is

affected and the splitting of the molecule is unbalanced. The production of free radicals occurs because radiation can only interact with one water molecule at a time so Equation 1.2 does not apply.

$$H_2O \rightarrow H_2 + O_2 \quad 1.1$$

$$2H_2O \rightarrow 2H_2 + O_2 \quad 1.2$$

Instead, a cascading effect of ROSs occurs within the cell as seen in Equation 1.3. Once a bond is broken, a hydroxyl radical is formed which is considered the most reactive byproduct. If it does not immediately interact with something else, hydrogen peroxide is created. And finally, a superoxide radical is formed before reacting once more to the stable oxygen molecule.

$$H_2O \xrightarrow{e^-} \cdot OH \xrightarrow{e^-} H_2O_2 \xrightarrow{e^-} O_2^- \cdot \xrightarrow{e^-} O_2 \quad 1.3$$

This process is increasingly more reactive if Iron is in the environment, causing a Fenton reaction where hydrogen peroxide interacts with Iron forming another Hydroxyl radical.

$$H_2O_2 + Fe^{2+} \rightarrow OH^- + \cdot OH + Fe^{3+} \quad 1.4$$

$$O_2^- \cdot + Fe^{3+} \rightarrow O_2 + Fe^{2+} \quad 1.5$$

These radicals readily damage DNA by causing chemical changes from the breakage of bonds. Speaking more generally, IR generates a spectrum of DNA and non-DNA lesions that both induce sensory proteins that can trigger repair mechanisms.

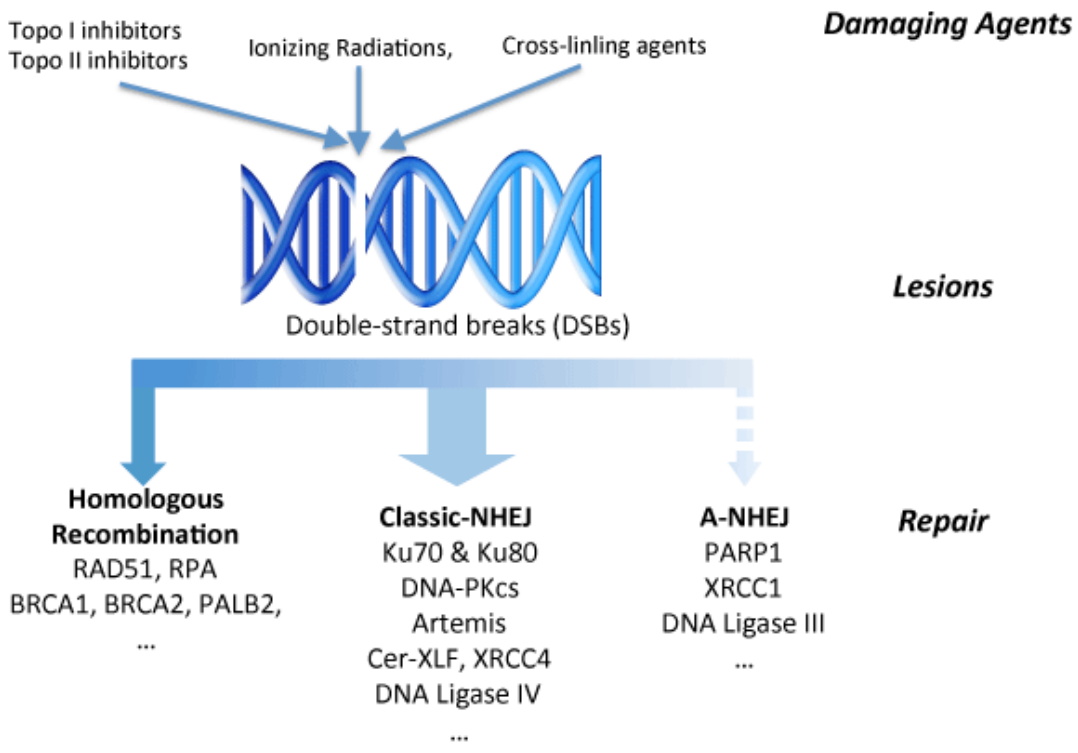

Figure 1-5 Repair Mechanisms after Double Strand Break in DNA (http://omicsonline.org/1948-5956/images/JCST-S8-001-g001.html) The image shows the potential causes of DSBs and the available repair processes along with the proteins involved with those processes.

When discussing damage to DNA, there are two types of concern: double strand breaks (DSBs) and single strand breaks (SSBs). Approximately, between 1 to 2 Gy, 1000 SSBs are and 40 DSBs are formed (Hall & Giaccia, 2012). DSBs are considered to be the most deleterious and are thought to trigger the most significant impacts in the cell's ultimate fate (Hall & Giaccia, 2012). Because damage from DSBs is significantly more complicated, more time is required for the cell to repair the damage. Therefore, as the dose rate increases, the more genotoxic stress is placed on the cell, and the more likely the cell will take drastic actions, such as apoptosis.

1.3.1 Cellular Response to Ionizing Radiation

Cells have evolved several mechanisms to sense and respond to cellular and genotoxic stress such as IR. Damage response differs by origin of cellular stress and can comprise of transcription factors, proto-oncogenes, signalling molecules and growth factors, as well as genes involved in response to tissue injury, inflammation and oxidative stress.

While DNA represents the critical target for the biological effects of IR, the responses generated after exposure can lead to activation of signal transduction cascade which in many cases activate critical transcription factors such as nuclear factor kappa-light-chain-enhancer of activated B cells (NFKB) or Tumor protein p53 (p53) (Criswell, Leskov, Miyamoto, Luo, & Boothman, 2003). As critical proteins involved in DNA repair and cell cycle arrest are regulated through protein level abundance this pathway might be an important determinant in cellular outcome (A. R. Snyder & Morgan, 2004). Exposure to IR can also lead to an increased release of cytokines and growth factors, allowing altered communication through these means (A. R. Snyder & Morgan, 2004).

The overall response to DNA damage is controlled mainly at the transcriptional level through regulatory elements. Changes in gene expression have been reported as fast as five minutes after irradiation and at doses of 10 cGy and below (Riecke, Rufa, & Cordes, 2012). The available data indicates that gene expression varies over time, beginning with the induction of “immediate early” transcriptional regulators and inflammatory response genes such as JunB, followed by the expression of secondary damage response genes controlling growth arrest and

DNA repair. The most relevant pathways involved in IR induced DNA damage repair seems to be Base excision Repair (BER) of single strand breaks and nonhomologous end joining (NHEJ) as well as Homologous Repair (HR) of double strand breaks (Dudáš & Chovanec, 2004; Reed, 2010) . However, these repair mechanisms may not account for other low dose cellular “nontargeted” effects such as “redox-sensitivity”, bystander effects (secondary effects on adjacent cells and tissues) and low dose hypersensitivity (Asur, Thomas, & Tucker, 2009).

High IR exposures can induce cell cycle arrest and apoptosis, particularly because of the increased number of DSBs being created. These effects can be caused through several pathways and involve many protein interactions and modifications (see Figure 1-5). The proteins ataxia telengiectasia mutated (ATM) and p53 are among the key players involved in mediating generalized IR responses (Hall & Giaccia, 2012; Pecorino, 2008). They work through multiple protein partners to affect an even larger number of unknown proteins and genes through various complex interactions suggesting that any absorbed radiation may have a biological effect by activating multiple pathways. Analyzing the modulation of these genes during IR exposure could bridge the gap between physical and biological dosimetry.

1.3.2 p53

P53 has a crucial role in abiding genomic integrity which is why this protein is often called “guardian of the genome” (Hall & Giaccia, 2012). It is important to realize though that the actual p53 dependent response to cellular stress depends highly on the cell type looked upon. In some cell types such as fibroblasts and epithelial

cells, p53 induces cell cycle arrest in the G1 and G2 phases of the cell cycle in order to prevent dissemination of DNA mutations to daughter cells. Depending on conditions such as DNA damage and cellular environment, the arrest in these cells can be permanent (resulting in growth arrest) or temporary (giving enough time for DNA repair and therefore the possibility to reenter cell cycle). However, in exquisitely radiosensitive cells (e.g. lymphocytes) p53 facilitates radiation induced apoptosis

Of all the activities of p53, none is more firmly accepted than the role of p53 as a transcription factor. Following DNA damage p53 can function as a transcriptional activator by binding to its consensus sequence within the promoter of target genes. P53 target genes can be classified into different groups according to their physiological roles. Some genes such as growth arrest and DNA-damage-inducible, alpha (GADD45A), the 14-3-3 protein zeta (14-3-3, or cyclin-dependent kinase inhibitor 1A (CDKN1A) are known to play a role in growth arrest, others play a role in cell cycle arrest, apoptosis, inhibition of angiogenesis or DNA repair (Amundson, 2008; Liu & Chen, 2002; Martinez et al., 2008). Some p53 regulated genes are known to create a so called “eat-me” signal in provoking potential elimination of damaged cells via the host-immune-response system through transcriptional regulation of for instance fractalkine or interferon regulatory factor 5 (IR5) (Schaue, Kachikwu, & McBride, 2012). This implies an essential role of p53 in immuno-surveillance to prevent cells from undergoing malignant transformation. p53 targets also include genes that can be linked to oxidative stress. Furthermore a large number of p53 target genes have been discovered that are involved in cell motility,

adhesion and migration and could therefore play a role in p53 mediated suppression of tumor metastasis.

1.3.2.1 Apoptosis

It has been suggested that p53 may play a role in apoptosis that is completely separate from the regulation of gene expression. It has been observed, that following stress p53 seems to function in the cytoplasm or at the mitochondria and that p53 can be found associated with several members of the BCL2 family (Cory & Adams, 2002; Zinkel, Gross, & Yang, 2006). p53 seems to be able to act as an “enabler," impeding the interaction between anti-apoptotic proteins such as B-cell CLL/lymphoma 2 (BCL2), BCL2-like 1 (BCLXL) and pro-apoptotic proteins. This could directly relieve the inhibition of the pro-apoptotic proteins BCL2-associated X protein (BAX) and BCL2-antagonist/killer 1 (BAK), or free BH3 only proteins such as BH3 interacting domain death agonist (BID) and BCL2-like 11 (BIM) which can then activate directly BAX and BAK.

p53 might also act as an “activator," activating BAX and BAK through binding and releasing them from anti-apoptotic proteins (Zinkel et al., 2006). Other proteins like BCL2 binding component 3 (PUMA) can then again displace p53 from binding anti-apoptotic proteins which also leads to apoptosis as PUMA now blocks the pro-apoptotic proteins and p53 is able to bind and activate pro-apoptotic proteins. Although under experimental conditions this transcription factor-independent activity of p53 alone can be sufficient for apoptosis, it seems probable that under physiological conditions this mitochondrial activity acts together with the role of p53

as a transcription factor. It has been suggested that the ability to accumulate mitochondrial p53 may be a distinguishing property between radio-resistant and radiosensitive organs and a determinant of whether or not a cell will die in response to p53.

1.3.2.2 Cell-Cycle Arrest

If a cell is capable of dividing, it will undergo a cycle of stages known as the Cell Cycle. There are four stages: G1, S, G2, and M. G1, S, and G2 are all considered part of the cycle called interphase. S phase is when DNA is replicated in the nucleus. And M phase is when mitosis occurs and the cell divides into two daughter cells. G1 and G2 are gap phases in between the S and M phases. There is also a G0 phase that occurs after the cell has become senescent.

There are three important check points in the cell cycle when considering the actions that the cell takes when undergoing any kind of stress. There is the G1 checkpoint, G2 checkpoint, and M checkpoint. Each of these checkpoints is a series of signaling pathways that are looking for DNA damage. When damage is sensed, Cyclin inhibitors bind with the appropriate CDKs and inactivate the progression into the next stage of the cell cycle (Pecorino, 2008). At the G1/S checkpoint, p21 (CDKN1A) inhibits cdk2 while at G2/M checkpoint GADD45A will inhibit cdk1 and prevent progressing into the M stage (Amundson, Grace, Mcleland, et al., 2004; Budworth et al., 2012; Martinez et al., 2008).

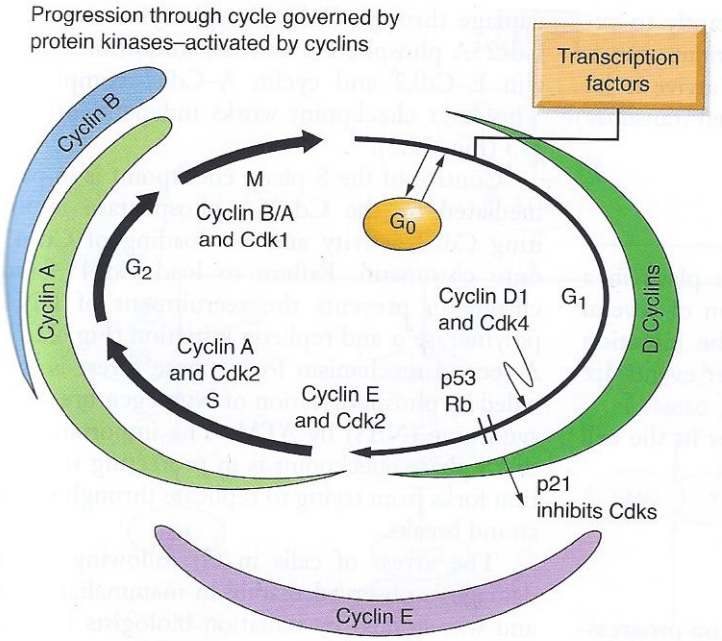

Figure 1-6 Progression through cycle governed by protein kinases-activated by cyclins

(Hall & Giaccia, 2012) See accompanying text for explanation of figure.

1.3.2.3 Repair Mechanisms

There are a few repair pathways that the cell can undergo when it senses damage to DNA. For SSBs, the DNA can undergo Base Excision Repair (BER) or Nucleotide Excision Repair (NER). In BER, the damaged base is removed and then replaced using the opposite base pair as a "recipe". DNA contains 4 bases that work in pairs: Adenine (A) pairs with Thymine (T) and Guanine (G) pairs with Cytosine (C). NER involves recognizing the damage to the base and bracketing a larger region than BER.

As said before, DSBs are much more complicated to repair. Immediately after sensing the damage, the cell cycle is arrested and ataxia telangiectasia mutated (ATM) kinase is activated. There are two processes of repair in competition at this

point: Homologous Recombination Repair (HRR) and Nonhomologous End-Joining (NHEJ). The difference between these two largely depends upon when in the cell cycle the damage to DNA occurs (Hall & Giaccia, 2012). If the cell is in G1, the cell will do NHEJ while if it is in late S/G2, the cell will do HRR. HRR is more reliable because in late S/G2, there is a sister chromatid that can be used to create a template for repair of the damaged section which in G1 there is no template available. Still, NHEJ has been found to occur in later S/G2 (Hall & Giaccia, 2012; Pecorino, 2008).

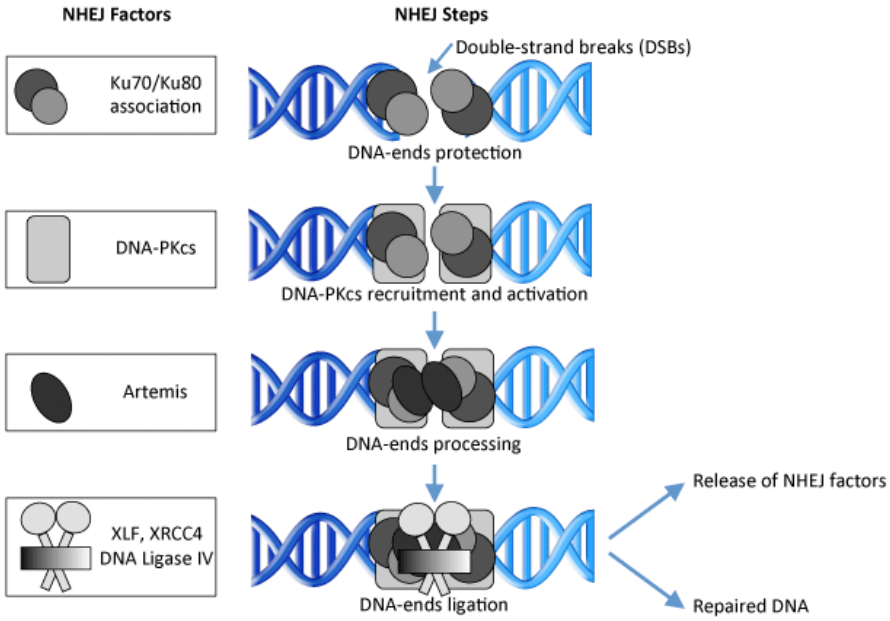

Figure 1-7 DNA Repair by NHEJ

(http://omicsonline.org/1948-5956/images/JCST-S8-001-g002.html) See text for explanation of figure.

NHEJ is error prone and the mutations are essential for creating antibody diversity (Hall & Giaccia, 2012). Damaged ends in a DSB site require modification

by proteins prior to being rejoined by ligation reactions. The exposed ends are recognized by Ku binding which then recruits DNA-dependent protein kinase catalytic subunits (DNA-PKcs). The ends are then processed with Artemis, another protein that forms a complex with the DNA-PKcs. The complex is then filled-in with bases (Hall & Giaccia, 2012).

1.4 Biodosimetry

Dosimetry is the method of measuring the amount of energy absorbed by a person from IR. This can be done through different methods. For external dose, dosimetry consists of wearing dosimeters that "capture" the energy from IR that can be analyzed later. There are also pocket dosimeters that read out the dose continuously while wearing it. These are used while working in radiation areas by nuclear industry, research, and medical personnel. For internal dose, though, there is no immediate way to read the dose one gets from an intake of radionuclides. Instead, doses are interpreted through bioassays, whether through urine or through fecal samples. This presents an issue in emergencies, such as a detonation of an improvised explosive device containing a radionuclide, or a "dirty bomb". During these situations, triage necessitates knowing who was exposed and to what extent there were exposed.

Biodosimetry is using biomarkers to determine the dose one receives from IR. There are three major approaches to biodosimetry. First, one can measure the biological changes from exposure to IR directly. Second, metabolic products can be modified by radiation and assays can be done to analyze these. Third, and the one of

focus, involves measuring the biological response to damage caused by IR (Swartz, Williams, & Flood, 2014). Regardless of what method is used, there are key criteria that must be met in order for biodosimetry to provide a benefit over traditional physical dosimetry:

Table 1.1 Key Criteria for Biodosimetry (adapted from Swartz et al., 2014)

1.	Be specific to ionizing radiation
2.	Have well-known effects by type of radiation and by dose rate
3.	Be unaffected by prior health status or concurrent perturbations such as wounds or stress
4.	Have a well-characterized dose–response that is either unaffected by individual variations or known for the type of individual being measured (e.g., based on gender)
5.	Reflect biological implications to the individual
6.	Have a constant or well-known response over the full period of relevant times
7.	Allow to provide results quickly
8.	Allow to be accomplished for the population at risk within the appropriate time frame
9.	Be suitable for the expertise that is likely to be available for the circumstances in which they will be used

Most genomic assays fulfill at least some of these criteria. Lymphocytes are used primarily because they are readily sampled and are some of the most radiosensitive cells in the body (Amundson, Bittner, Meltzer, Trent, & Fornace, 2001).

1.4.1 White blood cell based Biodosimetry

Many studies have been done to determine how different tissues and cells respond to IR and different methods have been developed for this very purpose. Of

the most widely used biomarkers used for biodosimetry are chromosomal aberrations after exposure to IR. The more common assays used to measure chromosomal aberrations are the dicentric assay and the micronucleus assay.

Dicentrics are formed by asymmetrical interchromosomal exchanges where the “sticky ends” of two broken centromeres reconnect prior to S phase. After S phase, this chromosome has two centromeres and is called dicentric (Hall & Giaccia, 2012). The formation of these dicentrics is linearly related to the radiation dose(Rana, Kumar, & Sharma, 2010). The practical lowest amount of dose in vivo detected is 0.5 Gy (Amundson et al., 2001; Rana et al., 2010). While this assay can reliably determine dose, specialized training is necessary and it can take a bit of time to do.

Figure 1-8 Dicentric Chromosome (http://usm.maine.edu/toxicology/chromium-toxicology-studies) Chromosome circled in red is an example of a dicentric chromosome.

Micronucleus assays requires less specialized expertise and are quicker. In this assay, lymphocytes are mitogenically stimulated in culture, then cytokinesis is blocked (the separation of one cell into two during mitosis). This results in mitosis

and nuclear division without cell division. Micronuclei are formed if there were any DSBs in the chromosomes. The left-over chromosomal fragments are unstable and form smaller structures in the cell that can be seen. Micronuclei are then counted in binucleated cells. Studies have shown that the number of micronuclei in binucleated cells increase linearly with dose (Amundson et al., 2001; Rana et al., 2010; Ropolo et al., 2012; Tucker, Vadapalli, et al., 2013). If fluorescence in situ hybridization (FISH) probes are used during this assay, the lowest dose measurable is thought to be 0.1 to 0.2 Gy (Amundson et al., 2001). Tucker et al. found that the lowest determinable dose was age dependent and increases linearly with age (Tucker, Vadapalli, et al., 2013).

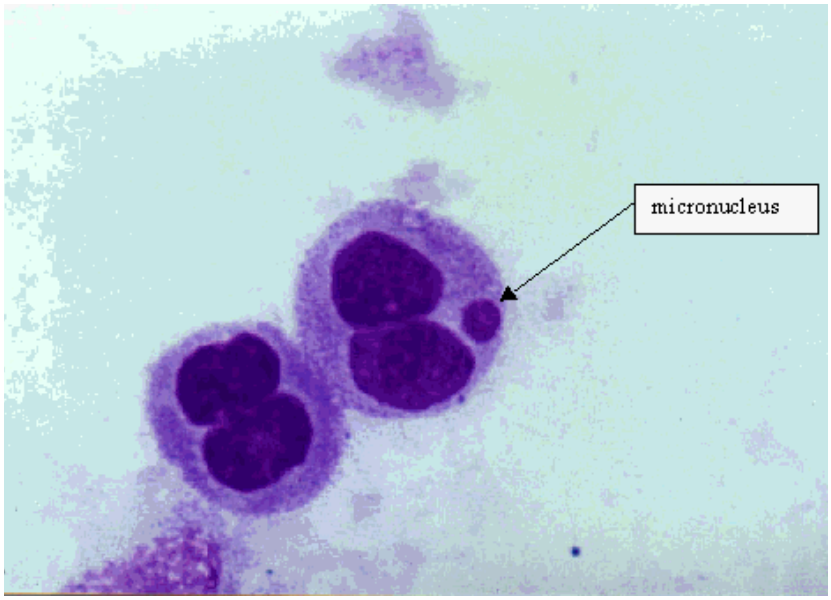

Figure 1-9 Micronucleus in Binucleated Cell (http://www.crios.be/genotoxicitytests/micronucleus_test.htm) Micronucleus is marked by the arrow in the above figure.

1.4.2 Gene Expression Biomarkers

Using gene expression as a biomarker for IR exposure is relatively new. As discussed earlier, gene transcripts are activated in response to IR exposure. The levels

of this activation can be measured to determine the extent that a gene is being expressed. Since the human genome is extremely large with approximately 20,000 to 25,000 protein-coding genes (Pray, 2008), techniques had to be developed that would look at a large number of genes at once. Two techniques commonly used for this purpose are serial analysis of gene expression (SAGE) and cDNA microarrays. Once genes are recognized as being important, real-time polymerase chain reaction (RT-PCR) can be conducted to target genes of interest.

1.5 Current Trends in Biodosimetry

Using RT-PCR for studies in biodosimetry is wanted due to its lower cost, its ease of conducting the analysis, and its reliability. After performing microarrays from lymphocytes and finding a smaller group of genes that are radiation-induced, researchers can target these genes with RT-PCR. Generally, genes in the p53 pathway have been targeted. These genes include cell-cycle arresters, DNA repairers, and apoptosis regulators.

In a 2004 study of patients undergoing total body irradiation (TBI), comparisons between *in vivo* responses and *ex vivo* responses of gene expression in peripheral white blood cells were made. CDKN1A and DDB2 were expressed but GADD45A, which had been known to be expressive, was not in this study (Amundson, Grace, & McLeland, 2004). This showed that the expression of GADD45A was complicated and others factors needed to be taken into consideration.

Because the p53 pathway is not only activated after exposure to IR, other confounding factors need to be taken into account when analyzing the results.

Budworth et al. found that CDKN1A, while definitely responsive to radiation, also responds to inflammation stress caused by bacterial endotoxin lipopolysaccharide. Other genes, though, were only activated to IR exposure (BBC3, FDXR, GADD45A, PCNA, XPC, POLH, and DDB2) (Budworth et al., 2012).

The behavior of the transcripts in the p53 network are not fully understood, therefore time after exposure has been taken into consideration in order understand this behavior. Tucker et al. exposed mice to different doses from a ^{60}Co source and obtained blood at different days after exposure. Using RT-PCR, they showed that CDKN1A expression was high at 0.5 days after exposure. CDKN1A also explained 50% of all variability in the multiple regression models used showing that the gene could be the primary variable in describing gene expression after IR exposure (Tucker, Divine, et al., 2013). Using this model, Tucker et al. exposed human blood ex vivo with a ^{60}Co source. They found that ASTN2 and CDKN1A together explained 84% of the variance in the multiple regression model used (Tucker et al., 2014).

1.5.1 Neuroblastoma Patients as a Model for Biodosimetry

^{131}I-mIBG provides an ideal opportunity to evaluate the clinical effects and mechanisms of radiation sensitizers. mIBG therapy uses radioactivity among the highest reported in this treatment-resistant population. Because hematologic toxicity is the main dose-limiting concern and^{131}I-mIBG rarely results in significant non-hematologic toxicity, this provides an opportunity to combine ^{131}I-mIBG with other systemic agents, particularly radiation sensitizers.

The current research focuses on CDKN1A as a prime candidate for determining dose, but it is difficult to determine whether the increased expression is due solely to IR exposure. In cancer patients, this is particularly concerning because patients are often treated with chemotherapy concurrently with radiotherapy. Also, most (if not all) studies use a dosimetry model based on external radiation sources, rather than internal sources which could be of more concern. This is not only because of TaRT, but also because of the high potential of an uptake during a radiological incident such as a reactor accident or detonation of a "dirty bomb".

The overall research approach of combining radiation sensitizers with a source of continuous radiation exposure represents a major innovation. Radiopharmaceuticals and brachytherapy provide continuous, rather than fractionated, radiation exposure to tumor cells. As such, data from studies using external beam radiation in combination with radiation sensitizers may not be directly comparable to studies utilizing sources of continuous radiation exposure.

Patients undergoing targeted radiotherapy provide a unique opportunity to model the effects of a radionuclide uptake on lymphocytes. Particularly, this study allows comparison between different environments of radiosensitizers provided by the randomized chemotherapy treatments. Analyzing the expression of genes within each patient can provide invaluable insight to the effects of internal radiation on lymphocytes and possibly the whole body. The aim of this thesis is to understand the mechanisms of gene expression during IR exposure and chemotherapy treatment and to develop a model that can predict the CEDE a patient receives based on modulation of key genes.

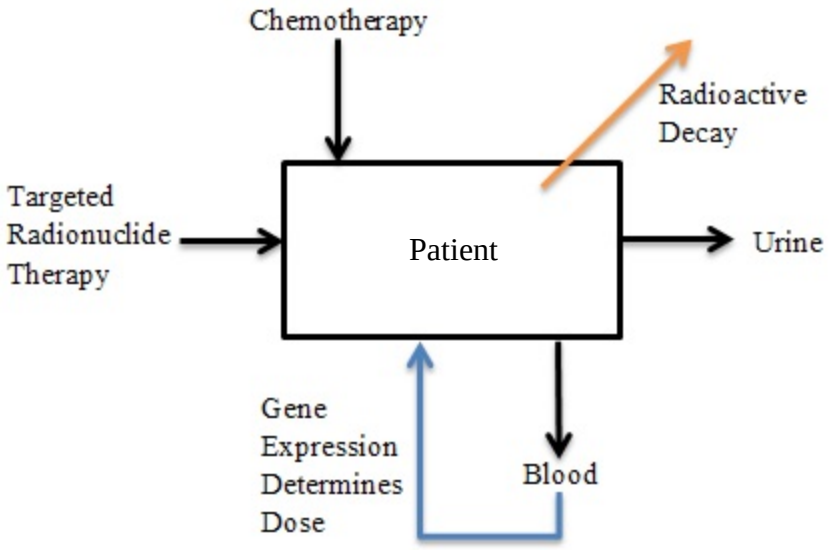

Figure 1-10 Model of Study In this study, the patient (as represented above by the box) has two therapies affecting him/her. Subsequently, the patient gives off radiation as the I-131 decays from the TaRT and also voids urine containing the radionuclide. Blood is sampled and the gene expression of the white blood cells is presumed to indicate the dose the patient received from the I-131.

2.0 MATERIALS AND METHODS

2.1 Patient Recruitment & Randomization

Patients were recruited from among the population of individuals with relapsed or refractory neuroblastoma evaluated at any of the 15 New Approaches to Neuroblastoma Therapy (NANT) locations, which include universities and children's hospitals in North America. Randomization was stratified according to potential predictors of response to ^{131}I-mIBG. This list of predictors included disease status (relapsed versus refractory disease), age at study entry (older than 18 years versus younger than 18 years), and bone marrow status at study entry (presence versus absence of bone marrow disease). Patients were assigned to one of the three ^{131}I-mIBG regimens at random, while balancing across the margins of each of the three stratification variables.

2.2 Blood Sample Retrieval

A total of 41 patients participated in the UCSF-led study. All patients had negative responses to their initial therapy with some having relapsed and other having poor responses to the initial therapy. All patients had MIBG-avid neuroblastoma found by performing ^{123}I-mIBG diagnostic scans. Patients were older than 24 months with a median age of 9 years. Prior to treatment, patients had foley catheters placed in their bladders prior to treatment as well as had their thyroids blocked to limit exposure from free Iodine during the treatment. Injection occurred over a 1 hour period within a lead-lined room at UCSF.

2.5 – 10 ml of peripheral blood was drawn using PAXgene RNA blood tubes at baseline, 72, 96, and some at 120 hours after treatment injection. For some patients, blood was drawn prior to treatment with chemotherapy and then another vial drawn prior to mIBG treatment. A total of 14 patients received mIBG treatment only, while 19 patients received Irinotecan and 7 received Vorinostat in combination with mIBG. 9 patients were deemed capable of receiving a second treatment approximately 6 weeks after initial treatment. After therapy, patients were discharged after radiation level at 1 meter from the body was less than 2 mrem/hr.

Blood tubes were kept at at -80 ºC at UCSF for 30 days after injection to ensure all ^{131}I has decayed away prior to shipping. Blood tubes were sent to Lawrence Livermore National Laboratory (LLNL) and then stored at -80 ºC until ready for RNA extraction.

2.3 IRB Informations

This study was approved by an Institutional Review Board at UCSF as well as LLNL under IRB Protocol #04-118 *Gene Expression Biodosimeters in Human Blood, Salive, and Buccosal Cells* at LLNL and IRB Protocol #11-05945 *Evaluation of Biomarkers of Radiation Exposure in Patients Treated with 131I-MIBG* at UCSF. All patients consented to genomic studies of gene expression and the study. Oregon State University was exempt from the IRB rules due to no physical involvement at OSU with the study.

2.4 Gene Selection for Biodosimetry

Genes listed in Table 2.1 were selected based on prior performance in previously conducted gene expression experiments (Amundson, Myers, & Fornace, 1998; Amundson, Grace, Mcleland, et al., 2004; Budworth et al., 2012; Sunirmal Paul, Smilenov, & Amundson, 2013; Wyrobek & Manohar, 2011). GAPDH was chosen as the reference gene. Most genes chosen were targets of the p53 activation pathway with a couple that were from different signal pathways. The apoptosis domain included FDXR, BBC3, BCL2, BCLXL, BAX, and BIM, while the Cell-cycle arrest domain included CDKN1A and GADD45A. The DNA repair domain was represented by XPC and DDB2.

Table 2.1 Selected Genes

Gene	*Name*	*Primer #*	*Description*
GAPDH	Glyceraldehyde 3-phosphate dehydrogenase	H202758991_g1	Glyceraldehyde 3-phosphate dehydrogenase is an enzyme of ~37kDa that catalyzes the sixth step of glycolysis, breaks down glucose for energy and carbon molecules
CDKN1A	Cyclin-dependent kinase inhibitor 1A (p21)	Hs0035578_m1	G1/S Cell-Cycle Arrest
FDXR	Ferrodixin Reductase	Hs00244586_m1	Apoptosis (Pro-apoptotic)
FLT3LG	Fms-Related Tyrosine Kinase 3 Ligand	Hs00957747_m1	Controls development of dendritic cells which provide adaptive immunity response to pathogens and priming pathogen-specific immune responses
GADD45A	Growth Arrest and DNA-damage-inducible, alpha	Hs00169255_m1	G2/M Cell-Cycle Arrest
DDB2	Damage-specific	Hs03044953_m1	DNA Repair, participates in

	DNA binding protein 2 (XPE)		nucleotide excision repair
BBC3	BCL2 Binding Component 3 (PUMA) P53 Up-regulated Modulator of Apoptosis	Hs00248075_m1	Apoptosis (Pro-apoptotic)
XPC	Xeroderma pigmentosum, complementation group C	Hs00190295_m1	DNA Repair, participates in nucleotide excision repair
MDM2	E3 Ubiquitin Protein Ligase	Hs00234753_m1	Inhibits p53, including inhibition of cell-cycle and apoptosis transcriptional activation domains.
NQO1	NAD(P)H Dehydrogenase, quinone 1	Hs02512143_s1	Member of NAD(P)H dehydrogenase family
BCL2	B-cell CLL/lymphoma 2	Hs99999018_m1	Apoptosis (Anti-apoptotic)
BCLXL	BCL2-like 1	Hs00236329_m1	Apoptosis (Anti-apoptotic)
BAX	BCL2-associated X protein	Hs99990001_m1	Apoptosis (Pro-apoptotic)
TP53I3	Tumor protein p53 inducible protein 3	Hs00153280_m1	Induced by p53. Involved in p53-mediated cell death.
STAT5B	Signal transducer and activator of transcription 5B	Hs00273500_m1	Member of STAT family of transcription factors that respond to cytokines and growth factors.
BIM	BCL2-like 11	Hs00708019_s1	Apoptosis (Pro-apoptotic)

2.5 RNA Preparation using PAX Gene Kit

In the Coleman Laboratory at LLNL, RNA was extracted from whole blood using a PAX Gene Kit (QIAGEN GmpH, Valencia, CA, USA) and the manufacturer's instructions. Prior to centrifuging, PAXgene vials are allowed to incubate at room temperature overnight to maximize RNA yield. After centrifuging, the nucleic acids are a pellet that is washed and resuspended in buffer. Proteinase K is

added to digest proteins. A shred spin column is used to homogenize the cell lysate and remove debris. Supernatant is transferred into a new microcentrifuge tube where ethanol is added to adjust binding conditions. RNA is bound to a PAXgene silica membrane. The membrane is then washed to remove remaining contaminants. DNase I is applied to the membrane to remove trace amounts of DNA. Final product is eluted with buffer and incubated at 65 °C for 5 minutes. RNA was stored at -80 °C until ready for use. RNA was quantified using a Nanodrop ND 1000 spectrophotometer (Nanodrop Technologies, Wilmington, DE, USA) and Qubit Fluormeter (Invitrogen, Carlsbad, CA, USA).

2.6 Synthesis of cDNA and Preamplification

For quantification using real-time PCR (RT-PCR) analysis, 200ng of RNA was converted to single-strand cDNA using the High Capacity cDNA archive kit (Applied Biosystems, Foster City, CA, USA). RNA was combined with buffer, enzyme mix, and RNase-free water. cDNA synthesis was conducted using a thermocycler. Incubation was done for 1 hour at 37°C then 5 minutes at 95ºC. cDNA was held at 4°C until removed and stored in a freezer between -15°C and -25°C.

cDNA was then pre-amplified with TaqMan PreAmp Master Mix(Applied Biosystems, Foster City, CA, USA). A pooled mix of TaqMan assay primers was combined with the preamp Master mix. 14 cycles of preamplification were done in a thermocycler. The cycles were 95 ºC for 10 minutes then 14 cycles of 15 seconds at 95 ºC and 4 minutes at 60 ºC.

2.7 Real-Time PCR

RT-PCR was used to quantify the expression of genes for each patient blood tube. Each reaction was performed in a volume of 20 µl and in triplicate to reduce error. A 96-well plate was used to run multiple reactions at once. In each well, pre-amplified cDNA was combined with water and 5x concentrated SharkaTAQ Stable QPCR Master Mix (Frontier Genomics, Auke Bay, AK, USA), and a single TaqMan primer from Table #. The plate was placed in a 7900 HT Fast Real-Time PCR System (Applied Biosystems, Foster City, CA, USA). The PCR program used was the following: 10 min at 95 °C, followed by 40 cycles of alternating 15 seconds at 95 °C and 1 min at 60 °C. Multiple 96 well plates were run for each primer. The computer analysed fluorescence using absolute quantification.

RT-PCR uses probe-based chemistry in order to discriminate between targeted and untargeted genes. The first 10 minutes were for annealing the TaqMan probe to the targeted gene sequence template on which the TaqMan probe from pre-amplification is bound. As the sample is cycled between 95 °C and 60 °C, the Taq polymerase degrades the probe, separating the reporter and quencher dyes, allowing the reporter to fluoresce. The intensity of the fluorescence increases in direct proportion to the amount of target cDNA synthesized and pre-amplified (Green & Sambrook, 2012).

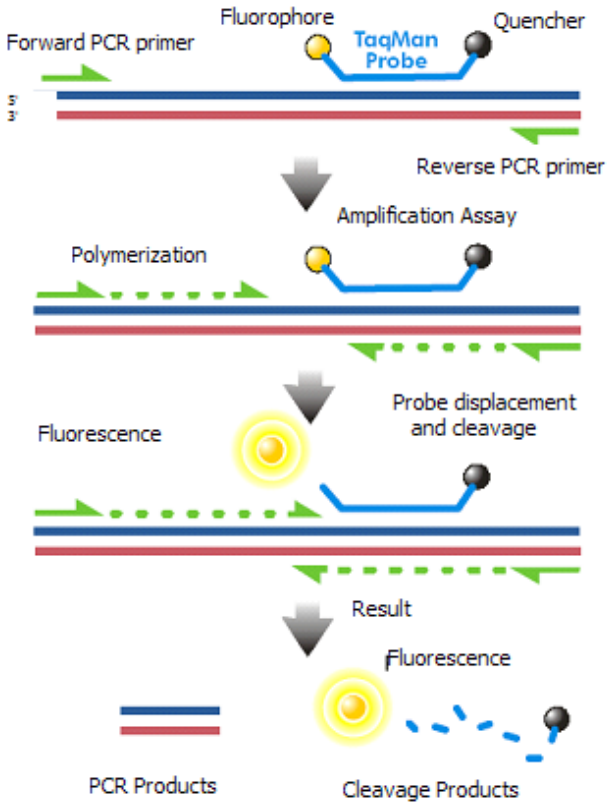

Figure 2-1 Diagram of RT-PCR using TaqMan probes (Figure is taken from http://upload.wikimedia.org/wikipedia/en/0/07/Taqman.png) The image shows the mechanism of how TaqMan probes work during RT-PCR. During the annealing phase, TaqMan probes attach to cDNA. As polymerization occurs, the fluorophore is cleaved off from the quencher and is allowed to fluoresce. Increasing amount of fluorescence is therefore proportional to the amount of that specific RNA contained within the sample.

2.8 Interpreting RT-PCR Results

RT-PCR produces an S-shaped curve that moves from exponential to quadratic. The point, or the number of cycles it takes, where the curve changes from exponential to quadratic is called the C_T value, or the Cycle Threshold. Analysis is done by comparing the C_T of each well. Triplicate samples are geometrically averaged to produce one value. Values can be further adjusted by using the $2^{-\Delta\Delta C_T}$

method described by Livak and Schmittgen by converting C_T to fold changes (Livak & Schmittgen, 2001). This allows different data sets to be compared.

$$\Delta C_{T(Target)} = C_{T(Target\ Time)} - C_{T\ (Target\ Baseline)} \quad 2.1$$

The ΔC_T of each target gene is the difference in cycle threshold between a specific sample and its baseline. It is calculated by using the geometric means of each time point and then subtracted from the geometric mean at baseline.

$$\Delta C_{T(GAPDH)} = C_{T(GAPDH\ Time)} - C_{T\ (GAPDH\ Baseline)} \quad 2.2$$

The ΔC_T of the reference gene, in this case GAPDH, is calculated the same way as the target gene.

$$\Delta\Delta C_{T(Target)} = \Delta C_{T(Target)} - \Delta C_{T(GAPDH)} \quad 2.3$$

The $\Delta\Delta C_T$ is calculated by subtracting the ΔC_T of the reference gene from the ΔC_T of the target gene. This takes into account any differences between times in the housekeeping gene because it is assumed that the housekeeping gene does not change from exposure to IR.

$$Fold\ Change = 2^{-\Delta\Delta C_{T(Target)}} \quad 2.4$$

The fold change is then calculated using the equation above. This number provides insight into how many times the amount of transcripts formed has duplicated during gene expression.

2.9 Statistical Methods

A variety of statistical tests were conducted to evaluate the data from RT-PCR. The analyses included Welch's T-Tests, multiple linear regressions, and step-

wise regression analyses. All analyses were conducted in the R environment (R Core Team, 2013). A P-value of 0.05 was used as the limit for statistical significance.

2.10 Internal Dosimetry

Absorbed dose was calculated using established methodologies common in the nuclear medicine field. For ^{131}I-mIBG treatments, various adjustments to the original method as describe by MIRD was necessary to compute reasonable doses due to the differences between the phantoms used and the younger and lighter children. ICRP 53 provided a background for the biokinetics of mIBG, many adjustments have been made based solely on the results in studies (Buckley, Chittenden, Saran, Meller, & Flux, 2009; Fielding & Flower, 1991; Flower & Fielding, 1996; Matthay et al., 2001; Monsieurs et al., 2001; Sudbrock et al., 2010).

2.10.1 Calculating CEDE based on ICRP Recommendations

Calculating the committed effective dose equivalent (CEDE) based on the ICRP model requires knowledge of the radionuclide decay scheme, the chemical behavior of the radionuclide in the body, and the residence time in each organ or compartment. To do this, the body is simplified into a series of compartments representing the different tissues and organs. There are schematics for inhalation and ingestion of radionuclides, but for the purposes of TaRT, injection is the most common mode of intake. Radiopharmaceuticals are injected into the blood which is also considered the transfer compartment because it travels to all locations in the body.

To determine the effective dose equivalent, dose equivalent must be first calculated for each tissue/compartment. To do this, the total number of nuclear transitions, or decays, must be calculated. Each radiopharmaceutical has two decay constants, one is the physical half-life that is determined by the radionuclide's properties, and the other is the biological half-life which is determined by the biochemical properties in the body. Each compartment will receive a percentage of the total amount of initial injected activity. Taking these variables into account, the activity is integrated over to determine the number of nuclear transitions in the compartment. It is a convention of the dose calculation methodology that the integration period is nominally set to 50 years. This approach captures the total number of radioactive decay transitions that are likely to occur during an individual's lifetime. For short lived radionuclides used in radiation therapy it encompasses essentially 100% of all decays that are likely to occur. The total number of decays which occur during this time is known as U_S. Equation 2.5 shows the way U_s is calculated where A_o is the initial amount of activity, λ_e is the effective decay rate constant, and *t* is time elapsed.

$$U_s = \int A_o(t) e^{-\lambda_e t}\, dt \qquad 2.5$$

For time 0 to *t*:

$$U_S = \frac{A_o}{\lambda_e}\left(1 - e^{-\lambda_e t}\right) \qquad 2.6$$

After the nuclear transitions are calculated, the radionuclide's radiative energies emitted during decay need to be taken into consideration. For beta emitters, the beta is considered (for all intents and purposes) to stay within the compartment. The energy per transitions is multiplied by the yield and divided by the mass of the

compartment. Gamma emission requires taking into account the absorbed fraction (AF) for the decays occurring within the compartment as well as those received from another compartment (also known as crossfire). Summation of all decay contributions in each compartment yields the specific effective energy (SEE) value. Equation 2.7 shows the calculation for SEE where Y_i is radiative yield, $\bar{E}_i$ is the average energy emitted per decay, $AF(T \leftarrow S)_i$ is the absorbed fraction from source to target tissue/organ, and m_T is the mass of the target tissue/organ (Martin, 2006).

$$SEE = \frac{\sum Y_i \bar{E}_i AF(T \leftarrow S)_i}{m_T} \quad 2.7$$

To get the CEDE ($H_{50,T}$), multiply the SEE and U_S by 1.6 x 10^{10} to convert from $^{MeV}/_{transition \times gram}$ to $^{J}/_{transition \times kg}$

$$H_{50,T} = 1.6 \times 10^{-10} \times U_s \times SEE(T \leftarrow S) \quad 2.8$$

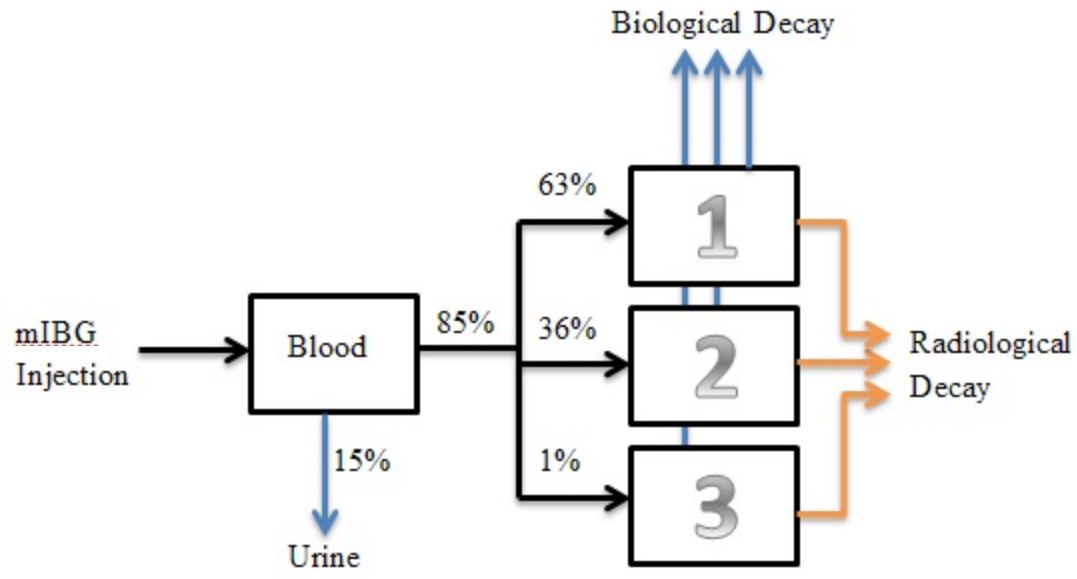

Figure 2-2 ^{131}I-mIBG Biokinetic Model This image shows the biokinetic model used for calculating dose in a patient undergoing ^{131}I-mIBG treatment. 15% of the original injection goes straight to the bladder and is removed. This leaves 85% to be distributed among mIBG-avid tissues in the body. 1% goes to the liver where it remains while the other 99% is shared in other tissues and decays through two compartments. Blue arrows represent biological decay and orange arrows represent radiological decay. Both are combined to give the effective decay rate for each compartment.

2.10.2 Absorbed Dose based on MIRD schema

The Medical Internal Radiation Dose schema was developed as a way for clinicians to calculate dose in the growing use of nuclear medicine for treatment and imaging. The calculation of dose using the MIRD schema is based on Equation 2.9 (Loevinger, Budinger, & Watson, 1991).

$$\bar{D} = \tilde{A}S(T \leftarrow S) \qquad 2.9$$

Ã (pronounced A-tilda) is calculated by integrating the number of nuclear transitions that occurs within a compartment and is effectively the same as the U_S in ICRP method described above. Its units are in “activity-time”, such as µCi-hour or MBq-hour. It can be calculated using Equation 2.5, or by the following:

$$\tilde{A} = 1.44 \times T_e \times A_o\left(1 - e^{-\lambda_e t}\right) \quad 2.10$$

S, called the S-Value, is the mean dose per unit cumulated activity and is calculated much the same as SEE. It is calculated by multiplying the number of radiations given off per decay (*n*) by the average energy of each radiation (*E*) and by the specific absorbed fraction ($\frac{\varphi}{m}$) where φ is the absorbed fraction (Loevinger et al., 1991).

$$S = \Delta\Phi \quad 2.11$$

Where: $\Delta = n\,E$ $\Phi = \frac{\varphi}{m}$ 2.12, 2.13

Such that: $S = \frac{nE\varphi}{m}$ 2.14

S-values are published (W. S. Snyder, Ford, Warner, & Watson, 1975) so generally there is no need to calculate the S-value, unless the affected person strongly deviates from the standard assumption of the schema.

2.10.3 Calculating Retention by Dose Rate

Another way to calculate total retention of activity in the body is by measuring the dose rate of a patient from a fixed position. At UCSF, a Victoreen 451 ion chamber detector was placed above the patient and was used continuously to monitor the dose rate from the patient, recording the measurement every 3 minutes. The rate of decay in the patient correlates directly with the rate of drop in dose rate read on the ion chamber. This information is saved and used to compare with the initial amount of activity injected into the patient.

2.10.4 Method of Dosimetry Employed at UCSF

Absorbed dose was calculated at UCSF utilizing the Medical Internal Radiation Dose (MIRD) models as well as by tracking dose-rates coming from the patient during treatment. The prescribed amount of ^{131}I-mIBG was injected into each patient over the course of an hour. During that time, 15% would be instantly removed to the kidneys and would exit the body through the catheter. After the one hour of injection, the "washout" begins. As defined at UCSF, the washout is the period of time it takes from completed injection to when the patient reads less than 2 mrem/hr at 1 meter. Absorbed dose was calculated using a two or three-compartment model for each patient which was then correlated with the dose-rates. In order to account for the difference S-values for each child versus the MIRD phantoms, the S-values were recalculated using Equation 2.16 where $m_{patient}$ is the mass of the patient.

$$S_{WB \leftarrow WB} = 1.34 \times 10^{-4} m_{patient}^{-0.921} \frac{Gy}{MBq \cdot hr} \qquad 2.16$$

2.10.5 Calculating Absorbed Dose at Different Time Points

Absorbed Dose was calculated by UCSF using the dose rate decay and the MIRD models as developed by the medical physicists. For this study, it was necessary to calculate absorbed dose at other specified time points in addition to the total amount received over the course of the treatment. To do this, a three compartment model was compared to the dose rate curve from 3 patients as supplied from UCSF. The effective decay constants for each compartment were averaged between the three patients. The resulting model was then used to compute absorbed doses at 72 hours, 96 hours, and 120 hours after injection.

3.0 RESULTS

3.1 Controls and patients with Neuroblastoma were obtained from UCSF

40 patients participated in this study coordinated by University of California San Francisco Children's Hospital. All patients were recruited and informed consent was obtained suing a consent form approved by their IRB. Neuroblastoma has a slight male predominance and, while enrollment was not based on sex, the study reflects this. There were 30 males and 10 females in the study group. Upon entry into the study, patients were chosen at random for each chemotherapeutic treatment in the study. 19 patients received Irinotecan and Vincristine, 7 patients received Vorinostat, and 14 patients only received mIBG. 17 patients in the study had their cancer relapse prior to treatment and 23 patients in the study had refractory cancer (did not respond to prior treatment). Nine patients in the study tolerated their first treatment well enough to have a second treatment within the same study. All of the patients agreed to provide whole blood under IRB numbers 11-05945 at UCSF.

Table 3.1 Summary of UCSF Patient Information

Number of Patients	40
Sex	Female: 10 Male: 30
Chemotherapy	Irinotecan + Vincristine: 19 mIBG Only: 14 Vorinostat: 7
Condition of Cancer prior to treatment	Relapsed: 18 Refractory: 22
White Blood Cell Counts	1st Treatment: 4.7 (units) SD = 2.5 2nd Treatment: 3.7 (units) SD = 1.6
Age	Average: 9.25 years Median: 7 years
Weight	Average: 31.2 kg avg. SD = 21.2
mIBG Activity	1st Treatment: 17.232 mCi/kg avg. SD = 1.5 2nd Treatment: 17.8 mCi/kg avg. SD = 1.2

3.2 Total RNA was isolated and converted to cDNA from patient whole blood

Whole blood was drawn and stored at -80 C in PAXGene tubes until shipped to LLNL. After the PAXGene kit was used and the RNA was isolated, RNA was measured using two methods: Spectroscopy with a Nanodrop Spectrometer and Fluoroscopy with a Qubit Fluorometer. Spectrometry with the Nanodrop looks for absorption at three different wavelengths, 230nm, 260nm, and 280nm. 260nm is generally what RNA and DNA absorb while absorption at 280nm indicated the presence of proteins. A high 260/280 ratio is greater than 2 and indicates a "pure" sample of RNA. On average, the first 26 patients and last 15 patients had high 260/280 ratios. Qubit uses fluorescent dyes for either of their targets, DNA, RNA, or protein. The specificity of the probes makes the Qubit fluorometer a more accurate measurement of RNA quantity.

Table 3.2 Summary of RNA Qualification

	First 26 Patients (Avg)	*All 41 Patients(Avg)*
RNA Yield	Nanodrop: 31.6 ng/ul Qubit: 27.6 ug/ml	Nanodrop: 43.87 ng/ul Qubit: 72.34 ug/ml
A260	0.79	1.09
A280	0.32	0.48
260/280	2.78	3.19
260/230	0.43	0.29

3.3 Doses were estimated using two different models

Cumulative effective dose equivalent (CEDE) was calculated initially at UCSF. Doses ranged from 43 cSv (Rem) to 541 cSv with a standard deviation of 105.8 cSv. These values were influenced directly by the patient's weight and amount of mIBG activity injected. UCSF doses are labeled "Model 1" in this study.

3.3.1 At LLNL a 3 compartment model was used to estimate dose

CEDE was also calculated at LLNL using a similar method but without the assistance of PRISM, called "Model 2" in this study. PRISM is software that takes the dose rate decay data from a patient and automatically calculates the retention function. Three patients' dose rate results from UCSF were examined to develop the retention function for all patients. Dose rates were obtained at UCSF every 3 minutes until the time when patient was removed from the treatment room. Dose rates were proportional to the amount of mIBG in the patient and the dose rate curve mimicked the retention function of the mIBG in each patient's body. Three patients' data were used to measure the retention function based on the rate of decay in dose rate from the patient.

Table 3.3 Biokinetic Model Compartments for Three Patients

	Compartment 1 $t_{1/2}$ *(hr)*	*Compartment 2* $t_{1/2}$ *(hr)*	*Compartment 3* $t_{1/2}$ *(hr)*
Patient 4	6.8	36	100
Patient 19	6.8	30	100
Patient 25	6	36	100
Average	6.53	34	100

Figures 3-1, 3-2, 3-3 show the differences between retention functions using Model 1 and Model 2. Using the averaged values in Table 3.4, as well as biokinetic information of mIBG in ICRP 53, Equation 3.1 was chosen as best fit for the model.

$$RF = \left[\left(0.36A_o e^{-\lambda_1 t}\right) + \left(0.63A_o e^{-\lambda_2 t}\right) + \left(0.01A_o e^{-\lambda_3 t}\right)\right] \quad 3.1$$

Equation 3.1 was used to calculate the absorbed doses at each time of blood draw at 72 hours, 96 hours, and 120 hours after injection. The integral of the retention function was multiplied by the calculated S-value for each patient based on patient's

weight. Doses ranged from 257 to 381 with a standard deviation of 27. Summary of CEDE data is in Table 3.3.

Table 3.4 CEDE Dosimetry Data

	Average	*Median*	*Range*	*SD*
mCi/kg	17.2	17.75	12.5 – 19.6	1.5
UCSF (Model 1)	263.1	234	43 – 541	105.8
LLNL (Model 2)	321.3	326.8	257 – 381	27

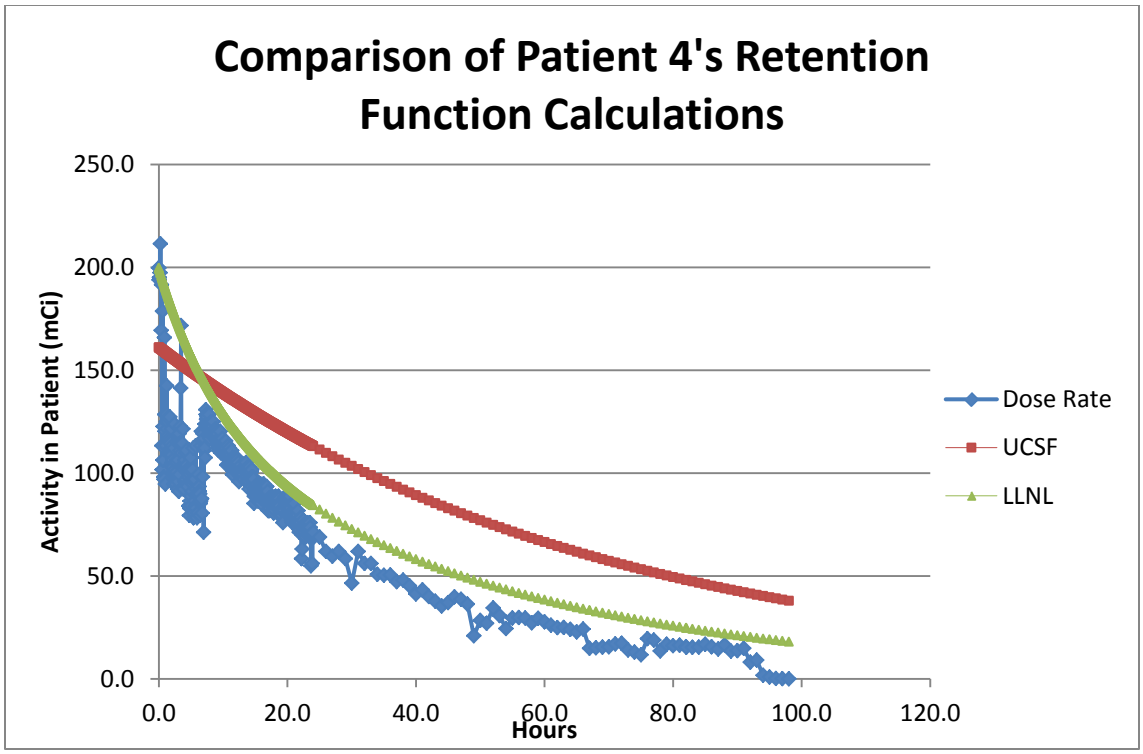

Figure 3-1 Comparison of Patient No. 4's Retention Function Calculations The blue line represents the dose rate as measured from the Victoreen 451 in the treatment room. The red line is the retention of mIBG as calculated by Method 1 and the green line calculated using Method 2. In this patient (No. 4), Method 2 follows the dose rate function much closer than Method 1. Method 1 was calculated using a two-dimensional function.

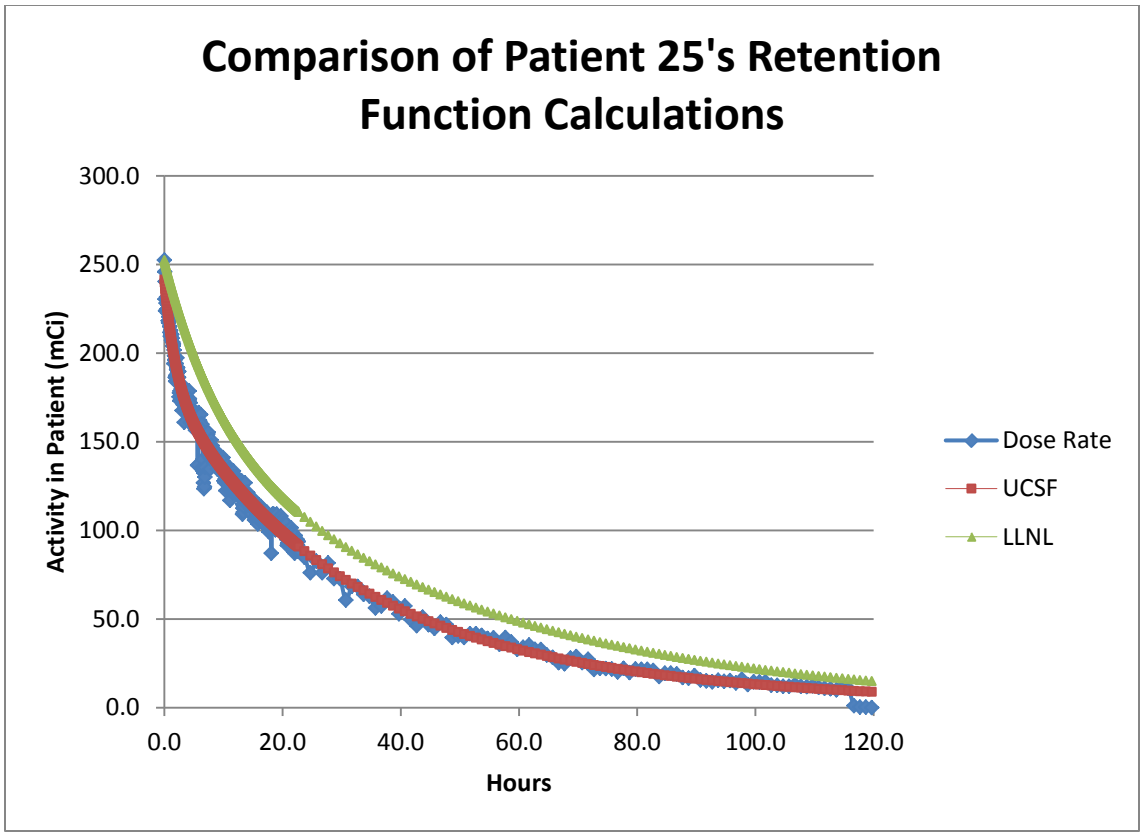

Figure 3-2 Comparison of Patient No. 25's Retention Function Calculations The blue line represents the dose rate as measured from the Victoreen 451 in the treatment room. The red line is the retention of mIBG as calculated by Method 1 and the green line calculated using Method 2. In this patient, Method 1 calculated the dose much more reliably due to it being a three-compartment model and the numbers were adjusted by PRISM much closer than the estimate from Method 2. Method 2 is still very close to the dose rate function.

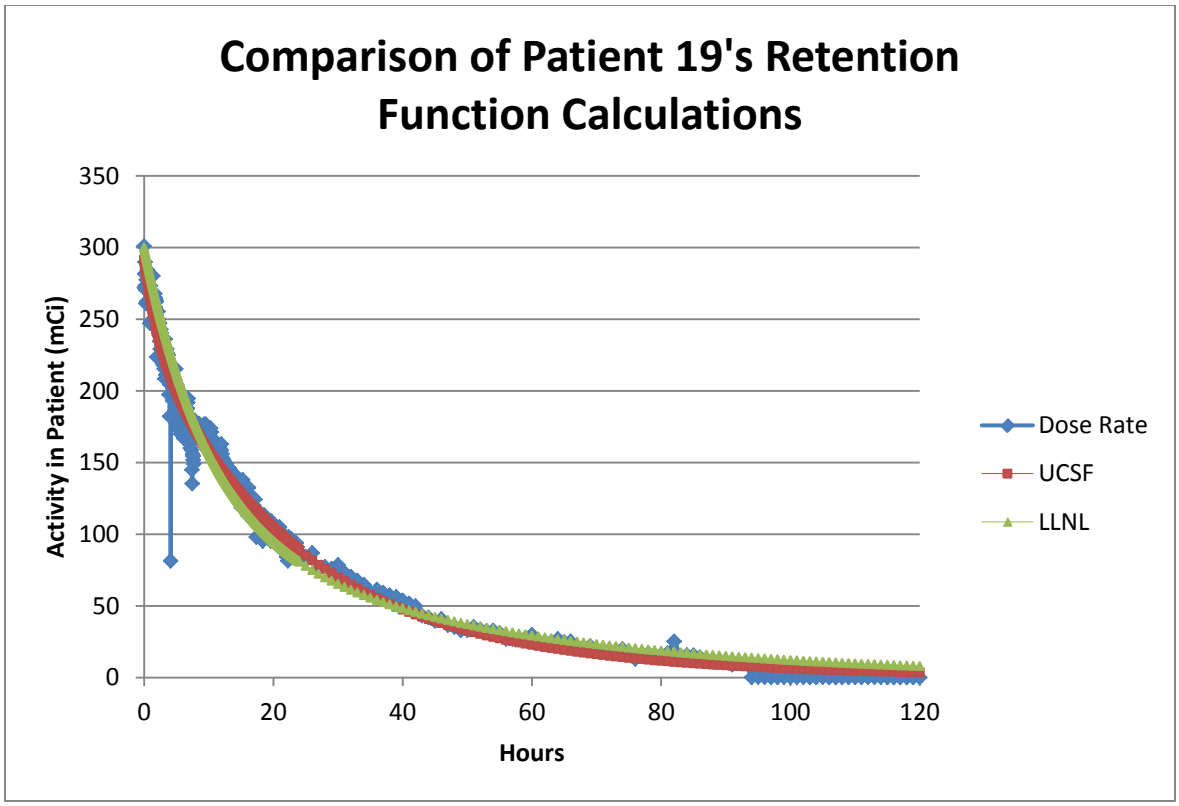

Figure 3-3 Comparison of Patient No. 19's Retention Function Calculations The blue line represents the dose rate as measured from the Victoreen 451 in the treatment room. The red line is the retention of mIBG as calculated by Method 1 and the green line calculated using Method 2. In this patient, both Method 1 and Method 2 tracked closely to the dose rate and either could be used for reasonable estimation of dose.

3.4 Identification of potential genes associated with IR exposure from mIBG

Initially, it was important to determine whether there were any gross differences in gene expression due to exposure to ^{131}I-mIBG. To determine this, Welch's two sample t-tests were performed to examine the response of each gene to the therapy. 11 genes (CDKN1A, FDXR, GADD45A, XPC, BCLXL, STAT5B, BAX, NQO1, DDB2, MDM2, and BIM) showed significant modulation in Log_2-transformed fold change between base time and 72 hours after injection of ^{131}I-mIBG. The same 11 genes showed significant modulation but less in magnitude between base time and 96 hours after injection. 7 genes (CDKN1A, FDXR, GADD45A, BCLXL, STAT5B, DDB2, and MDM2) were still significantly different between base time and 120 hours after injection.

Table 3.5 Summary of T-tests showing responses to radiation

	72 Hours		*96 Hours*		*120 Hours*	
	P-value	*DF*	*P-value*	*DF*	*P-value*	*DF*
CDKN1A	**<2.2E-16**	30	**1.258E-13**	27	**1.014E-06**	12
FDXR	**1.676E-14**	30	**1.806E-12**	27	**1.046E-05**	12
GADD45A	**9.958E-05**	30	**0.005218**	27	**0.01996**	12
FLT3LG	0.7486	12	0.7292	12	0.6488	4
XPC	**2.841E-06**	29	**1.985E-05**	26	0.2585	9
BCLXL	**0.001579**	29	**0.0002643**	26	**0.006997**	9
STAT5B	**0.00318**	29	**3.628E-05**	26	**0.01577**	9
BCL2	0.5411	29	0.9456	26	0.3998	9
BAX	**1.907E-07**	29	**2.315E-06**	26	0.4776	9
NQO1	**0.01076**	18	0.05304	15	0.614	4
DDB2	**8.22E-09**	18	**7.264E-05**	15	**0.009804**	4
MDM2	**0.009867**	20	**0.02991**	19	**0.02457**	11
BIM	**0.00106**	29	**0.001054**	26	0.1922	9

CDKN1A had the strongest response of all the genes at 72 hours and at 96 hours. FDXR was a close second. Both of these genes performed well at 120 hours, as well. For the most part, the responsive genes showed greater response between base

time and 72 hours than the other times with the exception of STAT5B and BCLXL. STAT5B had a much larger average response at 96 hours than at 72 hours ($p = 3.6E-05$), as did BCLXL ($p = 0.0003$). BIM had a nearly identical response between 72 hours and 96 hours.

3.4.1 Sex, weight, and age are potential confounding variables for differential gene expression

To assess whether other variables needed to be considered in the study, an analysis of confounding variables was done with a multiple regression analysis of each gene with sex, weight, age, and the condition of the patient's cancer prior to treatment. Most genes did not show any significant differences among any of these conditions. There were a couple of responses noted, though. GADD45A, BCLXL, and DDB2 had significant differences between male and female ($p < 0.05$). BCL2 had significant differences based on the patient's weight ($p < 0.05$) and patient's age ($p<0.01$).

Table 3.6 Confounding data for all patients

	Sex	*Mass*	*Age*	*Condition*
CDKN1A	0.12 (0.45)	0.007 (0.012)	0.03 (0.04)	0.21 (0.32)
FDXR	-0.5 (0.53)	0.008 (0.014)	0.005 (0.047)	0.18 (0.38)
GADD45A	**-1.47*** (0.65)	0.024 (0.018)	-0.028 (0.057)	0.79 (0.47)
FLT3LG	-1.49 (0.77)	-0.015 (0.012)	0.01 (0.05)	0.05 (0.61)
XPC	-0.23 (0.43)	-0.004 (0.01)	0.04 (0.036)	-0.13 (0.31)
BIM	-0.29 (0.34)	0.005 (0.009)	0.023 (.029)	0.06 (0.25)
BCLXL	**1.24*** (0.5)	-0.005 (0.012)	-0.05 (0.04)	-0.91 (0.36)
STAT5B	-0.62 (0.36)	0.008 (0.009)	0.04 (0.03)	0.33 (0.26)
BCL2	-0.19 (0.39)	**-0.02*** (0.01)	**0.09**** (0.03)	-0.31 (0.29)
BAX	-0.37 (0.3)	0.003 (0.007)	0.029 (0.025)	-0.23 (0.22)
NQO1	-0.65 (0.48)	0.006 (0.009)	0.04 (0.03)	0.52 (0.33)
DDB2	**-1.24*** (0.60)	-0.0002 (0.012)	0.07 (0.04)	0.41 (0.41)
MDM2	-0.25 (0.35)	0.02 (0.01)	-0.05 (0.04)	0.48 (0.33)

**** <0.0001, ***<0.001, **<0.01, *<0.05, + <0.1

3.4.2 Multiple Regression Analysis identifies subset of genes most useful for mibg treatment

Multiple regression analysis was conducted to assess the effects of IR, time elapsed from injection, and chemotherapy used. Because two models were used to estimate dose, two multiple regression analyses were run in tandem. Using doses supplied from UCSF, 6 genes (CDKN1A, FDXR, XPC, BAX, DDB2, and MDM2) showed significant responses at 72 hours; 7 genes (CDKN1A, FDXR, XPC, BCL2,

BAX, DDB2, and MDM2) showed significant responses at 96 hours; and 6 genes (CDKN1A, FDXR, XPC, BCLXL, DDB2, and MDM2) showed significant responses at 120 hours. The second model showed less significant findings with 4 genes (CDKN1A, FDXR, BAX, and DDB2) showing significant responses at 72 hours; 3 genes (CDKN1A, FDXR, and BAX) showing significant responses at 96 hours; and 1 gene (CDKN1A) being significant at 120 hours.

The strongest performing genes at each time point were CDKN1A and FDXR in respect to time after injection. CDKN1A had a strong average response of 2.29 ($p<0.001$) at 72 hours, 1.79 ($p<0.01$) at 96 hours, and 1.45 ($p<0.05$) at 120 hours. FDXR had a less strong, but significant average response of 2.29 ($p<0.01$) at 72 hours and 1.68 ($p<0.05$) at 96 hours. DDB2 response was significant at 72 hours with a response of 2.40 ($p<0.01$), 1.74 ($p<0.01$). BAX performed strongly at 72 and 96 hours with 1.48 ($p<0.05$) and 1.38 ($p<0.05$), respectively.

Patients treated with Irinotecan showed significant differences between themselves and those patients treated only with mIBG. 8 genes (FDXR, XPC, BIM, BCLXL, STAT5B, BCL2, BAX, and DDB2) had significant responses to the drug in comparison to mIBG only. BCLXL and BCL2 had the strong significant difference, but in opposite directions. BCLXL saw a significant down-regulation of 1.62 ($p<0.0001$) while BCL2 showed a significant up-regulation of 1.05 ($p<0.0001$) in gene expression.

Table 3.7 Model 1 – Multiple Regression Analysis Results

	Intercept	***Dose***	***72 Hours***	***96 Hours***	***120 Hours***	***Irinotecan***	***Vorinostat***
	β (SE)	*β (SE)*	*β (SE)*	*β (SE)*	*β (SE)*	*β (SE)*	*β (SE)*
CDKN1A	0.099 (0.15)	**-0.002*** (0.0009)	**3.08**** (0.27)	**2.64**** (0.28)	**2.49**** (0.36)	-0.16 (0.16)	-0.16 (0.21)
FDXR	-0.35 (0.19)	-0.0022 (0.0011)	**3.33**** (0.33)	**2.80**** (0.35)	**2.91**** (0.45)	**0.70***** (0.20)	0.17 (0.26)
GADD45A	-0.21 (0.41)	0.0045 (0.0025)	0.69 (0.72)	0.62 (0.76)	0.17 (0.99)	0.19 (0.42)	0.77 (0.57)
FLT3LG	0.203 (0.39)	-0.0008 (0.0039)	0.31 (0.93)	0.26 (0.97)	-0.14 (1.18)	0.102 (0.52)	**-1.57**** (0.54)
XPC	-0.43 (0.22)	**-0.003*** (0.001)	**1.83**** (0.39)	**2.03**** (0.42)	**1.50*** (0.57)	**0.86***** (0.23)	0.22 (0.34)
BIM	-0.28 (0.20)	0.00004 (0.0012)	0.67 (0.36)	0.91 (0.38)	0.498 (0.518)	**0.56**** (0.21)	0.11 (0.31)
BCLXL	**0.92**** (0.27)	-0.0009 (0.002)	-0.77 (0.47)	-0.91 (0.49)	**-1.67*** (0.68)	**-1.52***** (0.28)	**-1.59***** (0.40)
STAT5B	-0.25 (0.21)	**0.004**** (0.001)	-0.22 (0.36)	0.43 (0.38)	0.42 (0.53)	**0.53**** (0.21)	0.01 0.31)
BCL2	-0.32 (0.22)	**-0.004**** 0.001)	0.65 (0.38)	**0.95*** (0.40)	0.68 (0.55)	**0.94***** (0.22)	**-0.88**** (0.32)
BAX	-0.15 (0.16	-0.0015 (0.001)	**1.28**** (0.29)	**1.16**** (0.30)	0.67 (0.42)	**0.38*** (0.17)	-0.19 (0.25)
NQO1	-0.22 (0.31)	0.0006 (0.003)	0.63 (0.65)	0.85 (0.7)	0.007 (0.95)	0.33 0.35)	0.63 (0.48)
DDB2	-0.35 (0.25)	-0.002 (0.002)	**2.78**** (0.54)	**2.09**** (0.58)	**2.58**** (0.79)	**0.79*** (0.29)	-0.25 (0.40)
MDM2	0.02 (0.22)	-0.002 (0.001)	**1.10**** (0.39)	**1.14**** (0.4)	**1.26*** (0.50)	0.02 (0.23)	-0.15 (0.28)

****<0.0001, ***<0.001, **<0.01, *<0.05, + <0.1

Table 3.8 Model 2 – Multiple Regression Analysis Results

	Intercept	*Dose*	*72 Hours*	*96 Hours*	*120 Hours*	*Irinotecan*	*Vorinostat*
	β (SE)	*β (SE)*	*β (SE)*	*β (SE)*	*β (SE)*	*β (SE)*	*β (SE)*
CDKN1A	0.07 (0.18)	0.001 (0.002)	**2.29*** ** (0.56)	**1.79** (0.61)	**1.45*** (0.68)	-0.12 (0.17)	-0.15 (0.23)
FDXR	**-0.46*** (0.22)	0.002 (0.003)	**2.29** (0.69)	**1.68*** (0.75)	**1.56+** (0.84)	**0.82*** ** (0.21)	0.25 (0.28)
GADD45A	-0.24 (0.49)	0.001 (0.006)	1.41 (1.51)	1.38 (1.63)	1.22 (1.83)	0.15 (0.47)	0.85 (0.62)
FLT3LG	0.46 (0.54)	-0.002 (0.004)	0.56 (1.18)	0.54 (1.26)	0.21 (1.49)	-0.10 (0.51)	**-1.76** (0.62)
XPC	**-0.52+** (0.26)	-0.00007 (0.003)	1.24 (0.84)	1.40 (0.90)	0.61 (1.05)	**0.95*** ** (0.25)	0.28 (0.36)
BIM	-0.33 (0.23)	0.0008 (0.003)	0.50 (0.74)	0.73 (0.80)	0.29 (0.92)	**0.60** (0.22)	0.15 (0.32)
BCLXL	**1.07*** ** (0.30)	-0.00007 (0.004)	-1.03 (0.96)	-1.18 (1.03)	**-2.02+** (1.2)	**-1.62**** (0.29)	**-1.68*** ** (0.42)
STAT5B	-0.30 (0.25)	0.003 (0.003)	-0.09 (0.78)	0.56 (0.85)	0.76 0.98)	**0.55*** (0.23)	0.07 (0.34)
BCL2	-0.41 (0.26)	0.0008 (0.003)	-0.38 (0.82)	-0.14 (0.88)	-0.80 (1.03)	**1.05**** (0.25)	**-0.82*** (0.36)
BAX	-0.14 (0.19)	-0.002 (0.002)	**1.48*** (0.61)	**1.38*** (0.65)	0.83 (0.76)	**0.39*** (0.18)	-0.20 (0.26)
NQO1	-0.31 (0.39)	-0.0001 (0.003)	0.83 (0.97)	1.06 (1.05)	0.24 (1.30)	0.41 (0.38)	0.69 (0.52)
DDB2	-0.36 (0.33)	-0.0004 (0.003)	**2.40** (0.81)	**1.72+** (0.88)	**2.04+** (1.08)	**0.75*** (0.31)	-0.34 (0.44)
MDM2	-0.10 (0.26)	0.004 (0.003)	-0.27 (0.78)	-0.33 (0.83)	-0.45 (0.92)	0.13 (0.25)	-0.04 (0.31)

****<0.0001, ***<0.001, **<0.01, *<0.05, + <0.1

Patients treated with Vorinostat had only 3 genes (FLT3LG, BCLXL, and BCL2) significantly modulate compared to mIBG only patients. BCLXL had near the same magnitude of change as it did with Irinotecan. BCL2 reversed its response and was down-regulated by 0.82 ($p<0.05$) on average when the patient was treated with Vorinostat vs. Irinotecan.

3.5 CEDE was estimated using expression of selected genes as a model

Using the data from the first 26 patients, 6 genes were selected to develop a predictive biodosimetry model for neuroblastoma patients. CDKN1A was selected due to its strong responses as a cell-cycle inhibitor. BAX and FDXR were pro-apoptotic genes and had very strong responses. BCLXL was selected due to its discriminating performance between different chemotherapies. GADD45A was chosen because it has been shown to be a reliable biomarker for external radiation. STAT5B also had strong responses and its average behavior appeared to be inversely proportional to average BCLXL's behavior.

3.5.1 6 genes showed significant modulation in expression

After adding 15 patients, Welch's t-test were performed to assess if there was any change in modulation in bulk response to the therapy. Consequentially, there were greater significant differences between base time and 72 hours, as well as between base time and 96 hours. BCLXL and STAT5B both increased their significance when compared between 72 hours and 96 hours.

Table 3.9 T-Test Results of Response to Radiation				
	0-72 Hours		*0-96 Hours*	
	P-value	*DF*	*P-Value*	*DF*
CDKN1A	**<2.2E-16**	48	**<2.2E-16**	42
FDXR	**<2.2E-16**	48	**<2.2E-16**	42
GADD45A	**8.589E-09**	48	**1.604E-05**	42
BCLXL	**5.857E-05**	47	**6.889E-08**	41
STAT5B	**1.626E-06**	47	**4.747E-08**	41
BAX	**7.762E-12**	47	**2.305E-10**	41

3.5.2 Confounding analysis showed sex as a possible confounding variable

Re-assessment of confounding data was necessary to conclude whether the additional patients changed the effect of patient's sex, patient's weight, patient's age, and patient's cancer condition prior to treatment. For these 6 genes, GADD45A and STAT5B showed significant differences between male and female.

Table 3.10 Confounding Analysis for all 41 Patients (P-values)				
	Sex	*Mass*	*Age*	*Condition*
CDKN1A	0.95	0.87	0.67	0.31
FDXR	0.63	0.46	0.76	0.93
GADD45A	**0.03***	0.36	0.93	0.92
BCLXL	0.96	0.68	0.63	0.48
STAT5B	**0.006****	0.39	0.36	0.53
BAX	0.86	0.73	0.58	0.89

****<0.0001, ***<0.001, **<0.01, *<0.05, + <0.1

Additional confounding analyses were done to verify that prior treatments and chemotherapy alone did not alter the expression of genes in patients. Welch's two-sample t-tests were performed to judge whether there were changes in gene expression based on prior exposure from therapy. 6 patients received two therapies in this study. There were no significant differences found for all genes in these patients.

Five patients had two blood samples taken prior to treatment with ^{131}I-mIBG. The first was done prior to injection of chemotherapy and the second was taken just prior to ^{131}I-mIBG treatment. Welch's two-sample t-tests were also used to determine if chemotherapy has a lone effect on gene expression separated from exposure to ^{131}I-mIBG. There was no significant difference in gene expression due to chemotherapy alone.

3.5.3 Multiple Regression Analysis identifies significance of selected genes for modeling

Multiple regression analysis was performed to determine the effects of IR dose, elapsed time, and chemotherapy used on gene expression. All values used were transformed by taking the log2 of the fold change. As before, two separate multiple regression analyses were performed based on two different estimates of dose, doses provided from UCSF and doses calculated. Results differed significantly between the two groups. Generally, the difference in doses had no effect on the relationships

Table 3.11 Model 1 - Multiple Regression Analysis Results

	Intercept	*Dose*	*72 Hours*	*96 Hours*	*Irinotecan*	*Vorinostat*
CDKN1A	0.21 (0.13)	-0.0017* (0.0008)	3.16**** (0.23)	2.70**** (0.25)	-0.30* (0.14)	-0.43* (0.18)
FDXR	-0.26 (0.17)	-0.0019 (0.001)	3.39**** (0.29)	2.91 **** (0.31)	0.59*** (0.17)	-0.09 (.23)
GADD45A	-0.15 (0.29)	0.0038* (0.00018)	0.89 (0.49)	0.81 (0.53)	0.17 (0.30)	0.42 (0.39)
BCLXL	0.79*** (0.21)	0.0007 (0.001)	-1.31*** (0.37)	-1.56*** (0.4)	-1.34**** (0.23)	-1.10*** (0.31)
STAT5B	-0.18 (0.16)	0.002* (0.001)	0.38 (0.27)	0.78** (0.29)	0.39* (0.17)	-0.032 (0.22)
BAX	-0.15 (0.15)	-0.001 (0.0009)	1.49 **** (0.25)	1.41**** (0.27)	0.33* (0.15)	-0.02 (0.2)

****<0.0001, ***<0.001, **<0.01, *<0.05, + <0.1

At 72 hours and 96 hours, CDKN1A, FDXR, BCLXL, and BAX were significantly different from base time when all other variables were held constant. STAT5B was significant different for 96 hours. 72 hours after injection of ^{131}I-mIBG cause CDKN1A to increase by 2.73 ($p<0.01$), FDXR to increase by 3.51 ($p<0.01$), BCLXL to decrease by 3.37 ($p<0.05$), and BAX to increase by 3.43 ($p<0.01$). 96 hours after injection of ^{131}I-mIBG caused CDKN1A to increase by 2.23 ($p<0.05$), FDXR to increase by 3.03 ($p<0.05$), BCLXL to decrease by 3.79 ($p<0.05$), BAX to increase by 13.51($p<0.01$). The differences in expression between 72 hours and 96, on average were 0.5 for CDKN1A, 0.48 for FDXR, 0.42 for BCLXL, and 0.08 for BAX.

Table 3.12 Model 2 – Multiple Regression Analysis Results

	Intercept	*Dose*	*72 Hours*	*96 Hours*	*Irinotecan*	*Vorinostat*
CDKN1A	0.25 (0.15)	0.0002 (0.003)	2.73** (0.90)	2.23* (0.98)	-0.34* (0.15)	-0.48* (0.19)
FDXR	-0.26 (0.19)	-0.002 (0.004)	3.51** (1.13)	3.03* (1.23)	0.62** (0.19)	-0.11 (0.24)
GADD45A	-0.20 (0.33)	0.003 (0.007)	0.81 (1.95)	0.75 (2.12)	0.22 (0.33)	0.49 (0.42)
BCLXL	0.88*** (0.24)	0.008 (0.006)	-3.37* (1.49)	-3.79* (1.85)	-1.45**** (0.24)	-1.18*** (0.31)
STAT5B	-0.20 (0.18)	0.002 (0.004)	0.30 (1.13)	0.70 (1.23)	0.44* (0.18)	-0.006 (0.24)
BAX	-0.16 (0.16)	-0.009* (0.004)	3.43** (1.02)	3.51** (1.11)	0.35* (0.17)	-0.005 (0.22)

****<0.0001, ***<0.001, **<0.01, *<0.05, + <0.1

The addition of Irinotecan to the therapy caused significant differences in CDKN1A, FDXR, BCLXL, STAT5B, and BAX gene expression when all other variables were held constant. CDKN1A had a lower response of 0.09 ($p<0.05$) with Irinotecan while BCLXL has a much stronger decrease in gene expression response of 0.55 ($p<0.0001$). STAT5B had increased gene expression response of 0.21 ($p<0.05$) while FDXR had a strong response of 0.33 ($p<0.0001$). The addition of Vorinostat to the therapy causes significant differences in CDKN1A and BCLXL when all other variables were held constant. CDKN1A saw a decrease of 0.48 ($p<0.05$) and BCLXL saw a decrease of 1.18 ($p<0.001$).

3.5.4 GADD45A and BCLXL had significant interactions with increasing dose

An analysis of variance (ANOVA) was performed to look for interactions between absorbed dose, time after injection, and the chemotherapy used in conjunction with radiotherapy. Two genes had significant interaction terms.

GADD45A had a significant interaction between dose and time after injection (p = 0.002). BCLXL had a significant interaction between dose and chemotherapy used (p <0.0001).

Table 3.13 Summary of Results for Interaction Analysis (P-values)

	Dose	*Hour*	*Chemo*	*Hour*Dose*	*Chemo*Dose*
BCLXL	**2.43E-09**	0.06	**5.41E-09**	0.75	**2.78E-05**
GADD45A	0.70	**7.65E-06**	0.46	**0.003**	0.59

3.5.5 Step-wise Regression Analysis revealed a model that fit the patients' gene expression best

Using all parameters and using time as a continuous variable rather than a factor, step-wise regression was performed to determine which genes best describe the change in dose over time. The result of the regression showed that 4 gene responses and the time described 96% of the variance in dose across all patients. CDKN1A, FDXR, GADD45A, BAX and time after injection all contribute to describing the variance in the dose that a patient receives on average. This model would then be used to predict dose as a calibration equation (Equation 3.1).

Table 3.14 Parameters of Dose Calibration Equation

	Beta	*SE*	*P-value*
Intercept	6.57446	4.27803	0.1270
CDKN1A	16.70192	3.49499	5.17e-06
FDXR	6.86399	3.09547	0.0285
GADD45A	2.44853	1.53517	0.1134
BAX	-10.10926	3.93679	0.0115
Hour	2.40336	0.09775	<2e-16

$$E(Dose|CDKN1A + FDXR + GADD45A + BAX + Hour) =$$
$$6.57446 + 16.70192(CDKN1A) + 6.86399(FDXR) + 2.44853(GADD45A) -$$
$$10.10926(BAX) + 2.40336(Hour) \quad 3.1$$

3.5.8 Gene expression can be used to predict dose

The best-fit model was used to estimate absorbed doses on five patients based only on gene expression and time after injection of mIBG. These five patients had no dose information provided from UCSF besides mCi/kg injected into the patient for treatment. On average, the model estimated the dose within 7% of the calculated dose value. Thirteen out of 14 of the calculated doses were within the 95% prediction interval with 4 of them being within the 95% Confidence Interval for the gene expression model. The 72 hour calculated doses had a tendency to be further off from the predicted dose.

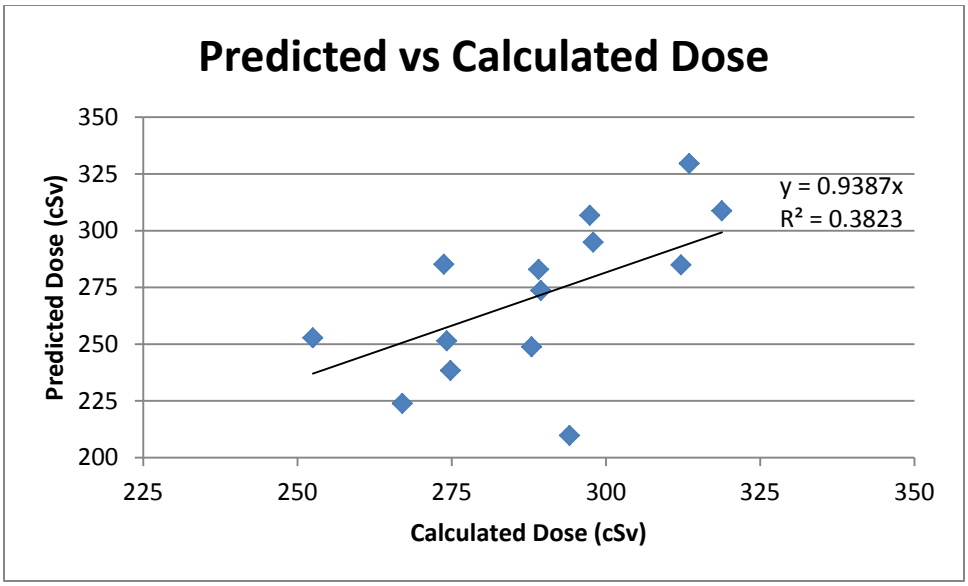

Figure 3-4 Predicted vs Calculated Dose This chart shows the correlation between predicted doses from the prediction equation in section 3.6 and the calculated doses from the Model 2 retention function. The values show a reasonably strong linear correlation.

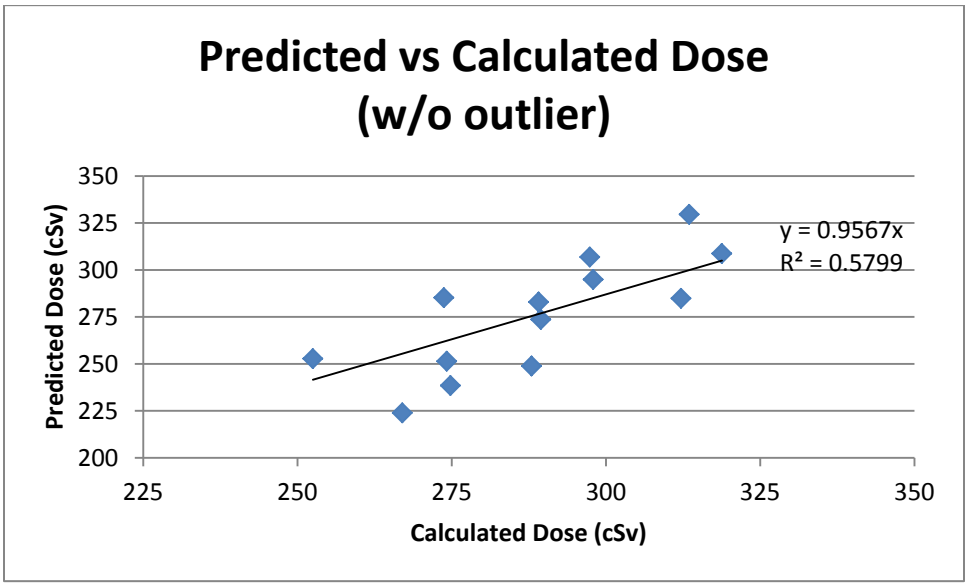

Figure 3-5Predicted vs Calculated Dose (without outlier) This chart shows the correlation between predicted doses from the prediction equation in section 3.6 and the calculated doses from the Model 2 retention function. Without the outlier, there is more linearity in the model with the relationship describe approximately 58% of the variability in the values.

Table 3.14 Predictive Model Results

	Hour	*Calculated Dose*	*Predicted Dose*	*95% Prediction Interval*	*95% Confidence Interval*	*% off from Calculated Dose*
13	72	274.81	238.42	183.2 – 293.66	226.4 – 250.45	15.26%
13	96	297.94	294.9	239.68 – 350.18	282.8 – 307.02	1.02%
13*	72	274.2	251.4	195.34 – 307.4	236.1 – 266.6	9.07%
13*	96	297.4	306.8	250.4 – 363.12	290.4 – 323.2	3.06%
15	72	267	223.9	167.6 – 280.12	207.87 – 239.9	19.25%
15	96	289.47	273.65	218.84 – 328.47	263.72 – 283.59	5.78%
31	72	289.1	282.91	226.04 – 339.79	264.79 – 301.04	2.19%
31	96	313.5	329.58	273.75 – 385.4	315.1 – 344.06	4.88%
32	72	252.5	252.76	197.68 – 307.8	241.49 – 264.02	0.10%
32	96	273.75	285.2	230.53 – 339.96	275.9 – 294.59	4.03%
33	72	294.1	209.79	154.36 – 265.22	196.92 – 222.67	40.19%
33	96	318.8	308.71	254 – 363.43	299.38 – 318.04	3.27%
40	72	287.95	248.84	194.15 – 303.53	239.64 – 258.03	15.72%
40	96	312.19	284.9	230.2 – 339.6	275.66 – 294.13	9.58%

4.0 DISCUSSION

4.1 Implications and design for comparing biological Dosimetry in neuroblastoma patients

By definition, absorbed dose is the amount of energy deposited per unit mass. In reality, dose is difficult to calculate without biological cues. When trying to conduct the longitudinal research on Japanese nuclear bomb survivors, dosimetry had to be estimated based on a person's memory of their position at the time of the detonation. Those doses were estimated based on the remembered location, distance from the detonation, and the topography of the locale. To say this is a difficult task would be understating it. Internal dosimetry has much the same difficulties. If anyone has a possible uptake from a radionuclide, unless a bioassay is taken, the dose is a rough estimate at best. Without a biological reference, whether it be urine or fecal activity content, estimating dose is just that, an estimate.

This makes internal biodosimetry research appealing because it can help develop techniques that can more precisely quantify the amount of absorbed dose one receives during incidents where uptake is a concern. In the medical field, estimating absorbed dose has been made relatively simple to undertake. Multiple methods can be employed to analyze the concentration of radionuclides in the body. In this study, whole body dose was estimated using the dose-rate decay as a representative of the body's retention function of mIBG. In other studies, imaging of the body using I-123-mIBG as the radionuclide has been used to great effect to measure the concentration of mIBG in different tissues of the body. This is particularly useful if there is a need to determine the dose to a specific organ.

Unfortunately, while imaging and examining patient dose-rate methods provide good information, they do not provide it for time-sensitive situations. There are other methods that can provide dose estimates closer to the time of exposure. Some techniques have already been used

to great effect, such as micronucleus and dicentric arrays, but these require specialized technicians and equipment. While these tests have linear responses to increasing dose, they are also expensive and take a significant amount of time. Genomic tests are of interest particularly because they are easier and cheaper to do. Potentially, PCR-style arrays can be done in a few hours and for a fraction of the cost. Genomic tests, with all of their benefits, have their own issues. While a lot has been learned about mechanisms of gene expression, there are many questions left unanswered that need to be approached. A lot of these frontiers can be seen in this study. First and foremost, these types of studies hinge on good dose estimates to begin with.

In this study, doses were estimated based on the dose-rate decay behavior of each patient after injection of I-131 mIBG. The retention factor was calculated based on ICRP 53 and studies that have looked into detail at the behavior of mIBG in the body. As described before, doses were calculated on a per-patient basis at UCSF using PRISM to automatically determine what the retention function is. In some patients, rather than a three-compartment model, a two-compartment model was used by the software which leads to dose estimates that were different than would be expected based on prior studies (Fielding & Flower, 1991; Flower & Fielding, 1996; Koral et al., 2008; Matthay et al., 1998, 2001). For the purposes of this study, instead of using PRISM, Microsoft Excel was used to trace the dose-rate decay curve and determine the retention function. Averaging the function over three patients provided a standardized way to estimate dose, but this approach lacks the patient-specific detail that can cause significant variances in the biokinetics of mIBG due to human variance. But, for the situations when the dose-rate curve is not reliable, whether it is because the patient moved dramatically or there was a fault in the instrument, a standardized curve prevents significant under or over estimation of dose.

The necessity of having a consistent and reliable dose estimation process is readily apparent in this study. Overall, two sets of multiple regression analyses were done using doses provided by UCSF and using the average retention function. Using the doses provided by UCSF, there were many significant findings as summarized in Table 3.7. The doses calculated by the average retention function, though, produced less significant findings, and those that were significant has lower P-values than those produced in the analysis using UCSF doses. The changes in significance can be summarized by the differences of standard error between the two analyses. Using UCSF doses, at 72 hours CDKN1A showed an increase in 3.08 with a p-value <0.0001 and standard error of 0.27 whereas in using the averaged retention function, CDKN1A showed a lesser increase of 2.29 with a p-value <0.001 and standard error of 0.56. There was also a moderate amount of evidence of a linear relationship between CDKN1A and increasing dose using the UCSF doses, while the averaged retention function did not have any significant evidence of the same linear relationship. Taking into account that the variance of the UCSF dose values between all patients was much higher than the averaged retention function, it appears that the variance was more assigned to the dose contribution, rather than to time. This becomes more pronounced when looking at the results for chemotherapies – the significance did not change by a whole lot between the two different approaches. While a lot of the patients had reliable dose-rate curves, the ones that did not obscured the results. Therefore, using the averaged retention function is more applicable for analyzing results.

There is a trade-off between using Excel to calculate an averaged retention function rather than using PRISM to determine dose to each patient individually. With access to each patient's dose-rate information, a clearer and more reliable dose can be assigned to the patient. But, because PRISM sometimes only calculates the dose using a two-compartment model, the

doses will be widely unreliable. For this reason, when calculating doses for developing a biodosimetry model, the benefits of using the averaged retention function outweigh the sometimes more accurate but unreliable doses calculated by PRISM.

4.2 Using mIBG patients as a model for estimating Dose to the Blood

Using peripheral white blood cells as a biodosimeter is the logical choice because blood goes everywhere in the body, but for beta-emitters (such as I-131) a lot of the dose is deposited in the blood, blood vessels, and the tumors, rather than anywhere else in the body. Therefore, using whole body dose as the measurement of comparison to gene expression might not be the best choice. That being said, it is difficult to model the dose to blood as self-shielding, flow dynamics, and continually changing blood vessel geometry affects the modeling (Hänscheid, Fernández, Eberlein, & Lassmann, 2014). But, by taking samples at regular intervals over a longer period of time (approximately 168 hours) and analyzing the activity concentration of mIBG in them, estimation of total activity in the blood and therefore dose can still be calculated. In 1956, A. A. Yalow conducted a study and derived an empirical equation:

$$D_{blood} = [0.214(B_1 - B_2)t_1] + (41.62B_2) \qquad 4.1$$

where t_1 is the effective half-life of mIBG retention in the blood (hrs) B_1 and B_2 are the concentration of mIBG in the first and lest measurements, respectively (Flower & Fielding, 1996). In Flower et al's study, they calculated a contribution of 0.04 to 0.17 mGy/MBq whereas in this study, it was calculated between 0.01 to 0.10 mGy/MBq with a range of doses to the blood of 0.95 Gy to 1.47 Gy. But, since the blood was never tested at 168 hours, nor was any blood tested for activity content, the dose estimates were not used for any calculations. But, if a

proper experiment was conducted, this could be a possibility for calculating dose and developing a biodosimetric model.

4.3 Biodosimetry Model based on Gene Expression

In order to use peripheral white blood cells as a biodosimeter, a complete understanding of p53's response to IR could be helpful. As explained, p53 activation contributes to three different mechanisms within the cell: cell-cycle arrest, apoptosis, and DNA repair. See Table 2.1 for further explanation of the genes chosen.

4.3.1 Dose-Dependent and Time-Dependent Gene Expression for Biodosimetry

Nearly all genes tested that were up-regulated and in this study showed a peak of expression at 72 hours with a slow decent of expression down to 120 hours. This behavior can also be seen in a recent study by Tucker et al. with careful examination of the changes in CDKN1A ΔCt for 2.5 Gy at 1 day vs 2 days (Tucker et al., 2014). Based on this study and Tucker's study, there are two behaviors of gene expression that need to be accounted for in models. First is the dose-dependent response where greater dose causes more expression of that gene. As has been shown in studies, CDKN1A particularly appears to increase in expression linearly with increasing dose until it reaches a threshold around 6 Gy and plateaus off exponentially (Tucker et al., 2014; Tucker, Divine, et al., 2013; Wyrobek & Manohar, 2011). This particularly affects dose prediction because doses greater than 6 Gy cannot be predicted with certainty (Tucker, Divine, et al., 2013).

The second behavior of concern is the time-dependent response where with greater time elapsing after exposure, the expression of the gene should dampen. To make this more

complicated are the effects of an exponentially decreasing source of radiation that is persistent rather than acute. It could be argued that this type of situation is more likely with the uptake of radionuclides being a concern for nuclear accidents and “dirty bomb” detonations.

Comparing the T-test results to the multiple regression results, a discrepancy can be noted. For the first 26 patients, there are significant differences between the times and baseline for CDKN1A, FDXR, GADD45A, XPC, BCLXL, STAT5B, BAX, DDB2, MDM2, and BIM. But, in the multiple regression analysis, only CDKN1A, FDXR, BAX, DDB2, and BCLXL showed significant differences between baseline and time. The genes that did not remain significant in the multiple regression analysis were influenced by the introduction of chemotherapy into the analysis. XPC and BIM both had strong significant differences between mIBG-only therapy and therapy using Irinotecan.

4.3.2 p53 responsive genes as a Model for Response to Ionizing Radiation

Classifying the gene expression within cells after exposure to IR is of the upmost importance when trying to decide upon a model that best reflects the amount of energy deposited in a given system. To this point, internal dosimetry and molecular biology are linked. As can be seen, then IR is incident upon a white blood cell, a host of p53-dependent genes are activated, as well others in other response pathways. While the p53 pathway appears to hold great promise as a great predictor of dose, it is possible that other pathways such as JNK and FAS could be used as well. In this study, two segments of the p53 pathway were looked at by targeting genes that are known to arrest a cell’s cycle as well as ones that are known to induce (or protect against) apoptosis.

4.3.2.1 Cell-Cycle Arrest

CDKN1A (or p21) is a critical target of p53 once p53 is activated. It encodes CDK1 which renders cyclin and Cdk complexes inactivated, thus leading to an accumulation of hypophosphorylated Rb proteins. In such a state, Rb is unable to break its association with transcription factors such as E2F which means E2F responsive genes cannot be activated and the cell cannot move into S phase. In this way, CDKN1A acts as a checkpoint for the G1/S phase (Somasundaram & El-Deiry, 2000). In studies using in vitro models, CDKN1A was also shown to bind with PCNA, blocking DNA replication (Somasundaram & El-Deiry, 2000). CDKN1A has been shown to be a very robust and highly significant response gene to ionizing radiation exposure (Amundson et al., 1998; Amundson, Grace, Mcleland, et al., 2004; Budworth et al., 2012; S Paul & Amundson, 2008; Tucker et al., 2014; Tucker, Vadapalli, et al., 2013).

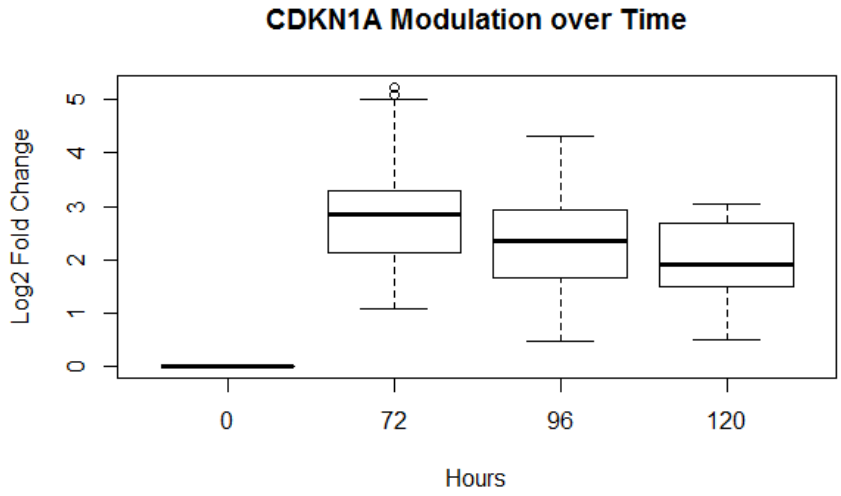

Figure 4-1 CDKN1A Modulation over Time CDKN1A reaches a peak average value at 72 hours and its modulation decays over time.

CDKN1A has a strong increase in fold change after exposure to IR. In this study, CDKN1A showed the strong increase in fold change, but did not show a significant change in

fold change with increasing dose. There is one reason for this that can be seen in this study, compared to others. As time lapses after an initial exposure, each cell undergoes critical decisions after CDKN1A halts cell cycle progression. Cells can repair themselves, undergo apoptosis, or become senescent. And, even though accumulated absorbed dose is increasing over time, the dose rate is decreasing. In this study, time after exposure becomes a stronger factor in determining the amount of CDKN1A expression in white blood cells after 72 hours of exponentially decreasing exposure.

From a systems point-of-view in this study, CDKN1A expression is a combined result of the amount of dose received and the time elapsed since initial exposure. CDKN1A has shown to increase in modulation with increasing dose (Amundson et al., 1998; Amundson, Grace, Mcleland, et al., 2004; Tucker et al., 2014; Tucker, Divine, et al., 2013) and in this study, time after initial exposure shows to decrease the amount of expression. Combining previous results with the results in this study, it appears that CDKN1A's expression is a polynomial curve generated by two competing functions of dose and time after exposure. The peak of the curve is depending on the initial dose-rate and then the shape of the decay is depending on time and decay rate of the dose-rate.

GADD45A is another p53 target gene that activates the G2/M cell cycle checkpoint inhibiting the activity of CyclinB1/Cdc2 complex. In other studies, GADD45A had strong responses after exposure to IR. Budworth et al. found that GADD45A increased strongly 24 hours after exposure to 2 Gy (Budworth et al., 2012). Paul and Amundson found that GADD45A had a dose-response signature in microassay experiments using patients undergoing TBI, but did not find a signature in peripheral blood lymphocytes (Amundson, Grace, Mcleland, et al., 2004; S Paul & Amundson, 2008). The results in this study showed that GADD45A did not respond

with any dose-effect just as Amundson noted in 2008. GADD45A expression also did not appear to be significant in regards to time as well. But, when including an interaction term, GADD45A showed a strong interaction between time and dose.

4.3.2.2 Apoptosis

The BCL2 family is a group of genes that form proteins that regulate apoptosis, whether through inducing or inhibiting it. This study looked at four genes (BCL2, BCLXL, BIM, and BAX) initially, before looking at BAX and BCLXL for the entire set of patients. After DNA damage occurs during IR exposure, p53 is directly localized to the mitochondria where is interacts with members of the BCL2 family. BAX and BCLXL oppose one another when induced by cellular stress. BCLXL suppresses apoptosis by sequestering cytoplasmic p53. Nuclear p53 then transcribes PUMA which binds to BCLXL and displaces p53 so that it can directly activate BAX, which promotes apoptosis (Zinkel et al., 2006). This balancing act determines whether a cell has determined to live or die. After BAX is activated, it induces mitochondrial permeabilization by oxidizing the mitochondrial pores, leading to cytochrome c release (Zinkel et al., 2006). BAX alone, though is not enough for radiation-induced apoptosis, there are more factors (Amundson et al., 1998).

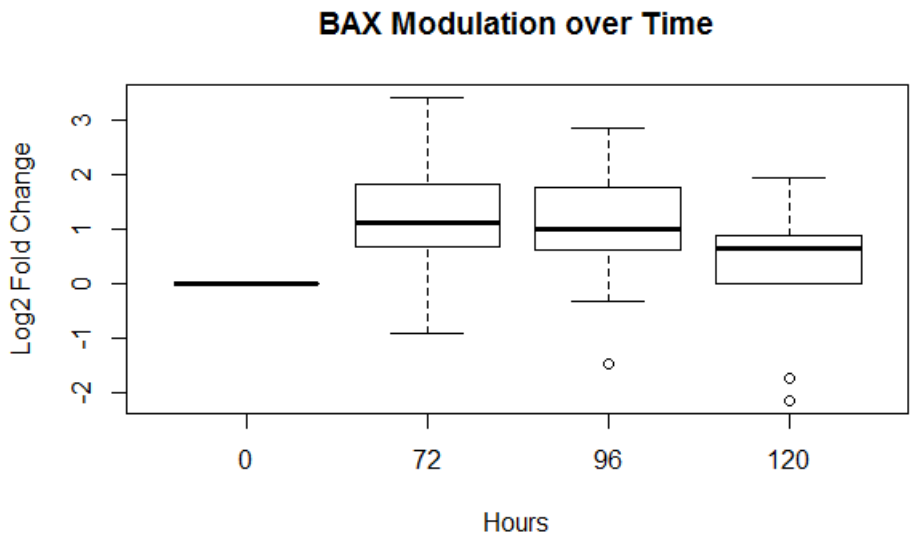

Figure 4-2 BAX Modulation over Time BAX reaches a peak average value at 72 hours with a decay as time increases.

In this study, BCLXL was down-regulated significantly at 72 hours after injection while BAX was up-regulated significantly. This shows that the population of white blood cells in the samples was more likely to, on average, undergo apoptosis rather than stay alive. BCLXL was one of the few genes to have a strong effect as time passed while undergoing the treatment with the average response increasing its down-regulation significantly. This could represent that damage to the DNA was so severe that even after halting the cell cycle, the damage was unrepairable and so the average response was to still undergo apoptosis. This would mean that a sustained IR dose over time would still have an effect on cells.

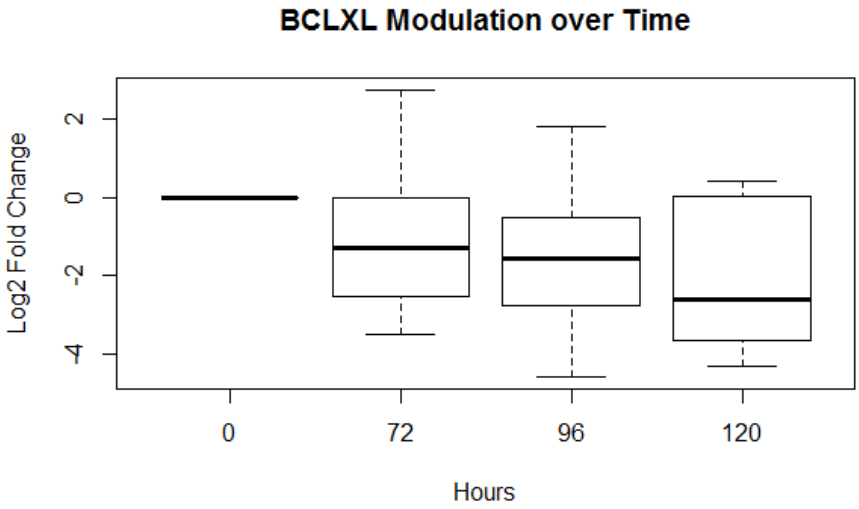

Figure 4-3 BCLXL Modulation over Time BCLXL shows to have a decline in value signifying an increasing down-regulation of the gene over time.

FDXR creates a protein called FR that is involved with the electron transfer from NADPH to cytochrome P450 in the mitochondria (Knops et al., 2012). FDXR is activated by p53 once cellular stresses induce Reactive Oxygen Species (ROS). These ROS, which were described earlier as having a strong effect on DNA, may also cause oxidation of mitochondria pores. This may upset the membrane potential and lead to a release of cytochrome c – the end result of the caspase cascade that eventually leads to apoptosis. This could also be caused by the synthesis of FR, the protein product of FDXR, which sensitizes cells to ROS-mediated apoptosis (Liu & Chen, 2002).

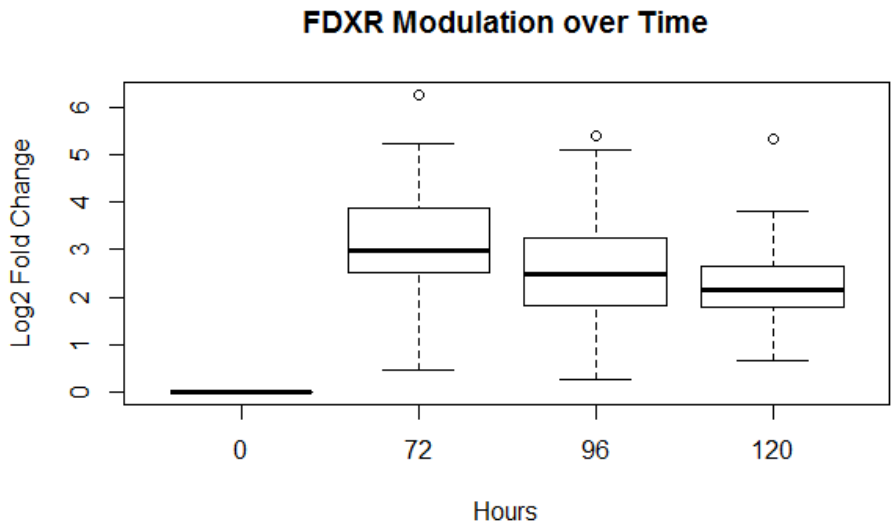

Figure 4-4 FDXR Modulation over Time FDXR shows a very strong peak at 72 hours where it decays off.

Because FDXR appears to directly lead to apoptosis, the amount of FDXR produced is likely directly proportional to the number of cells undergoing apoptosis within a sample. While the BCL-2 family could be metaphorically a game of tug-and-war between apoptosis and anti-apoptosis forces, FDXR either bypasses this game completely, or is a representation of who is winning. FDXR had the same response pattern as CDKN1A, with a peak value at 72 hours and a lower one at 96 hours. But, FDXR's fold increase was larger than CDKN1A's possibly showing that the dose-rate exhibited by the mIBG was inducing an apoptotic bias on the cells.

4.3.3 Internal exposure from mIBG as a model for biodosimetry

In this study, 4 genes were selected by a stepwise regression to represent the overall behavior of the data in response to increasing dose. Including time in the function was necessary because there were obvious differences in the genes' responses at 72 hours and 96 hours. The function is empirical and based solely on the values in this study and so could only possibly be

used in another neuroblastoma study with similar patients and absorbed doses. Even with that limitation, there is a lot to be understood by looking at the model. The values in the empirical model are weighed contributions to the final dose estimate. Because the model is based on mIBG radiotherapy, absorbed dose increases over time therefore the contribution of time to the model is logical. CDKN1A, FDXR, and GADD45A have been shown to increase based on increasing prompt dose and in this study also show to have non-zero fold changes as absorbed dose accumulates over time. BAX has a negative coefficient in the model which could represent a couple ideas. One, it might take time for the BCL-2 Family to determine whether to transcript for apoptosis or survival functions. Two, BAX has multi-domain functions involving cell-cycle arrest and apoptosis decisions (Zinkel et al., 2006), therefore with increasing dose (and subsequent increasing DNA damage), BAX is less likely to promote moving from G1 to S phase. So, in summary, the model is saying that increasing dose causes more cell-cycle arrest, more apoptosis, less proliferation, and less survival.

Table 4.1 Summary of Gene Modulation over Time in Study

	72 Hours	*96 Hours*	*120 Hours*
CDKN1A	↑↑	↑↑	↑↑
FDXR	↑↑	↑↑	↑↑
GADD45A	↑	↑	↑
BCLXL	↓↓	↓↓	↓↓
BAX	↑	↑	↑
STAT5B	↑	↑	↑

4.4 Future Direction

While the knowledge of genomics is increasing every day, many knowledge gaps still exist in regards to gene expression. We know that CDKN1A as very responsive to IR exposure and studies have shown that its increase in behavior is close to linear with increasing dose. But these studies only deal with acute doses. This would be useful for determining doses from total body irradiation therapy and possibly criticality accidents, but for targeted radiotherapy or nuclear accidents, these studies are less useful. Instead, a study like this one is needed that takes into account the exponential decay of activity after an uptake of a radionuclide. In this study, CDKN1A had a peak at 72 hours and subsequent decay to 96 and 120 hours (as did FDXR and most other genes in the study).

While this study takes great strides towards developing a biodosimetry model, there are aspects that cannot be controlled for, particularly because of a lack of knowledge in the area. It does not need to be explained further, but human beings are complex animals and at the genomic level, there are greater levels of complexity that are yet to be understood. One example of this complexity is the bystander effect where unexposed cells adjacent to exposed cells inexplicably also die (Asur et al., 2009; Morgan & Bair, 2013; Schaue et al., 2012). One possible cause for this is that the death of a cell from IR causes cytokines to be released into the intercellular fluid, which are then taken in by healthy cells and then undergo apoptosis (Schaue et al., 2012). Cytokines are also released for other reasons, such as oxidative stress, bacteria, viruses, and the list goes on. With evidence of this intercellular communication, each individual sample could be drastically changed by unknown variables in the patient.

While genes in this study represent good IR-responsive genes, there are possibly better ones out that, or at least better combination of genes to use in a model. Preferentially, a good model will have as few genes as possible and as consistent of responses as possible. In the situation of radiotherapy patients, a gene's expression that directly represents the max dose rate and a gene's expression that directly represents the time that has elapsed since the max dose rate occurred. This could also be useful in the case of an uncontrolled release of radioisotopes. If the radioisotope is known, then the biokinetic model is also and therefore, this model could be used as well to determine the dose to an exposed person.

Fold change was used as the comparing tool in this study, but the ΔC_T value would be a better estimate. There were some benefits for using fold change rather than just the ΔC_T values. As can be seen in Table 3.1, the raw RNA yields for the first 26 patients were a lot less and so, the raw C_T values would be different between the first 26 patients and the last 15. So, to compensate for that, fold changes allow for normalization of the data based on its comparisons to time and the normalization housekeeping gene, GAPDH. The downside of this strategy is that in order to calculate a fold change, one must have a base value. In the case of a nuclear incident, the base value would be unknown and so the fold change model would not work.

One of p53's mechanisms was not explored in this study. None of the selected DNA repair genes proved to be significant over time and therefore were not used in developing the model. And as microarray studies have shown, there are a lot of other genes besides p53 responsive genes that are responsive towards IR exposure. Other systems could be as important, and potentially more important, to describe biological effects of radiation.

5.0 CONCLUSION

In summary, this thesis shows that biodosimetry models can be created to predict absorbed dose based on blood-based gene expression. Even when taking into account the different environments of radiosensitivity within the patients, a model could predict a dose that was at worse within 40% and at best a fraction of 1%. This thesis also shows the importance of a proper dosimetry model for patients when evaluating the predictability of a model. Future work still needs to be done to understand the possible confounding factors that may still be yet to be discovered, relationships that have not yet been realized. Further studies utilizing targeted radiotherapy patients will not only help us develop methods for personalizing treatment for enhanced therapeutic results, but will also help us better understand effects of ionizing radiation at the molecular level. In the end, this could provide a stronger knowledge basis for radiation protection.

Appendix A

International Neuroblastoma Staging System & Proposed Neuroblastoma Risk Groups (Adapted from Wolden, 2007)

	Description	*Low Risk*	*Intermediate Risk*	*High Risk*
Stage 1	Localized tumor with complete gross excision, with or without microscopic residual disease; representative ipsilateral lymph nodes negative for tumor	All	None	None
Stage 2A	Localized tumor with incomplete gross excision; representative nonadherent lymph nodes negative for tumor microscopically	Age <1 yr Age 1-21 yr; MYCN nonAMP	None	Age 1-21 yr; MYCN AMP; UH
Stage 2B	Localized tumor with or without complete gross excision, with ipsilateral, nonadherent lymph nodes positive for tumor. Enlarged contralateral lymph nodes must be negative microscopically	Age 1-21 yr; MYCN AMP; FH		
Stage 3	Unresectable unilateral tumor infiltrating across the midline, with or without regional lymph node involvement; or localized unilateral tumor with contralateral regional lymph node involvement; or midline tumor with bilateral extension bt infilatration (unresectable) or by lymph node involvement	None	Age <1 yr; MYCN nonAMP Age 1-21 yr; MYCN nonAMP; FH	Age 0-21; MYCN AMP Age 1-21 yr; MYCN nonAMP; UH
Stage 4	Any primary tumor with dissemination to distant lymph nodes , bone, bone marrow, liver, skin, and/or other organs (except as defined in stage 4S)	None	Age <1 yr; MYCN NonAMP	Age <1 yr; MYCN AMP Age 1-21 yr
Stage 4S	Localized primary tumor (as defined for stage 1, 2A, or 2B) with dissemination limited to skin, liver, and/or bone marrow (limited to infants <1 years of age)	MYCN nonAMP; FH, DI>1	MYCN nonAMP; UH	MYCN AMP MYCN nonAMP; DI=1

References

Amundson, S. A. (2008). Functional genomics in radiation biology: a gateway to cellular systems-level studies. *Radiation and Environmental Biophysics*, *47*(1), 25–31. doi:10.1007/s00411-007-0140-1

Amundson, S. A., Bittner, M., Meltzer, P., Trent, J., & Fornace, a J. (2001). Biological indicators for the identification of ionizing radiation exposure in humans. *Expert Review of Molecular Diagnostics*, *1*(2), 211–9. doi:10.1586/14737159.1.2.211

Amundson, S. A., Grace, M. B., Mcleland, C. B., Epperly, M. W., Yeager, A., Zhan, Q., … Fornace, A. J. (2004). Human In vivo Radiation-Induced Biomarkers : Gene Expression Changes in Radiotherapy Patients Advances in Brief Human In vivo Radiation-Induced Biomarkers : Gene Expression Changes in Radiotherapy Patients, 6368–6371.

Amundson, S. A., Grace, M., & McLeland, C. (2004). Human in vivo radiation-induced biomarkers Gene expression changes in radiotherapy patients. *Cancer Research*, *64*, 6368–6371. Retrieved from http://cancerres.aacrjournals.org/content/64/18/6368.short

Amundson, S. A., Myers, T. G., & Fornace, a J. (1998). Roles for p53 in growth arrest and apoptosis: putting on the brakes after genotoxic stress. *Oncogene*, *17*(25), 3287–99. doi:10.1038/sj.onc.1202576

Asur, R. S., Thomas, R. a, & Tucker, J. D. (2009). Chemical induction of the bystander effect in normal human lymphoblastoid cells. *Mutation Research*, *676*(1-2), 11–6. doi:10.1016/j.mrgentox.2009.02.012

Buckley, S. E., Chittenden, S. J., Saran, F. H., Meller, S. T., & Flux, G. D. (2009). Whole-body dosimetry for individualized treatment planning of 131I-MIBG radionuclide therapy for neuroblastoma. *Journal of Nuclear Medicine : Official Publication, Society of Nuclear Medicine*, *50*(9), 1518–24. doi:10.2967/jnumed.109.064469

Budworth, H., Snijders, A. M., Marchetti, F., Mannion, B., Bhatnagar, S., Kwoh, E., … Wyrobek, A. J. (2012). DNA repair and cell cycle biomarkers of radiation exposure and inflammation stress in human blood. *PloS One*, *7*(11), e48619. doi:10.1371/journal.pone.0048619

Chabot, G. (1997). Clinical pharmacokinetics of irinotecan. *Clinical Pharmacokinetics*, *33*(4), 245–259. Retrieved from http://link.springer.com/article/10.2165/00003088-199733040-00001

Cory, S., & Adams, J. M. (2002). The Bcl2 family: regulators of the cellular life-or-death switch. *Nature Reviews. Cancer*, *2*(9), 647–56. doi:10.1038/nrc883

Criswell, T., Leskov, K., Miyamoto, S., Luo, G., & Boothman, D. a. (2003). Transcription factors activated in mammalian cells after clinically relevant doses of ionizing radiation. *Oncogene*, *22*(37), 5813–27. doi:10.1038/sj.onc.1206680

DuBois, S. G., & Matthay, K. K. (2008). Radiolabeled metaiodobenzylguanidine for the treatment of neuroblastoma. *Nuclear Medicine and Biology*, *35 Suppl 1*, S35–48. doi:10.1016/j.nucmedbio.2008.05.002

DuBois, S. G., & Matthay, K. K. (2013). I-131 Metaiodobenzylguanidine therapy in children with advanced neuroblastoma. *Quarterly Journal of Nuclear Medicine and Molecular Imaging*, *57*(1), 53–65.

Dudáš, A., & Chovanec, M. (2004). DNA double-strand break repair by homologous recombination. *Mutation Research/Reviews in Mutation Research*, *383*(6), 873–892. doi:10.1016/j.mrrev.2003.07.001

Fantin, V., Loboda, A., & Paweletz, C. (2008). Constitutive activation of signal transducers and activators of transcription predicts vorinostat resistance in cutaneous T-cell lymphoma. *Cancer Research*, *68*(10), 3785–3794. doi:10.1158/0008-5472.CAN-07-6091

Fielding, S., & Flower, M. (1991). Dosimetry of iodine 131 metaiodobenzylguanidine for treatment of resistant neuroblastoma: results of a UK study. *European Journal of …*. Retrieved from http://link.springer.com/article/10.1007/BF02285457

Flower, M. A., & Fielding, S. L. (1996). Radiation dosimetry for therapy of neuroblastoma Radiation dosimetry for neuroblastoma I-mIBG therapy of. *Physics in Medicine and Biology*, *41*, 1933–1940.

Green, M. R., & Sambrook, J. (2012). *Molecular Cloning: A Laboratory Manual* (4th ed.). New York: Cold Spring Harbor Laboratory Press.

Hall, E. J., & Giaccia, A. J. (2012). *Radiobiology for the Radiologist* (7th ed.). Philadelphia: Lippincott Williams & Wilkins.

Hänscheid, H., Fernández, M., Eberlein, U., & Lassmann, M. (2014). Self-irradiation of the blood from selected nuclides in nuclear medicine. *Physics in Medicine and Biology*, *59*(6), 1515–31. doi:10.1088/0031-9155/59/6/1515

ICRP. (1988). Radiation Dose to Patients from Radiopharmaceuticals. *Annals of the ICRP*, *ICRP Publi*(1-4).

Knops, K., Boldt, S., Wolkenhauer, O., & Kriehuber, R. (2012). Gene expression in low-and high-dose-irradiated human peripheral blood lymphocytes: Possible applications for biodosimetry. *Radiation Research*, *178*(4), 304–312. doi:10.1667/RR2913.1

Koral, K. F., Huberty, J. P., Frame, B., Matthay, K. K., Maris, J. M., Regan, D., … Yanik, G. a. (2008). Hepatic absorbed radiation dosimetry during I-131 metaiodobenzylguanidine (MIBG) therapy for refractory neuroblastoma. *European Journal of Nuclear Medicine and Molecular Imaging*, *35*(11), 2105–12. doi:10.1007/s00259-008-0873-3

Kushner, B., Kramer, K., & Modak, S. (2011). High-dose cyclophosphamide–irinotecan–vincristine for primary refractory neuroblastoma. *European Journal of Cancer*, *47*, 84–89. doi:10.1016/j.ejca.2010.09.014

Liu, G., & Chen, X. (2002). The ferredoxin reductase gene is regulated by the p53 family and sensitizes cells to oxidative stress-induced apoptosis. *Oncogene*, *21*, 7195–7204. Retrieved from http://europepmc.org/abstract/MED/12370809

Livak, K. J., & Schmittgen, T. D. (2001). Analysis of relative gene expression data using real-time quantitative PCR and the 2(-Delta Delta C(T)) Method. *Methods (San Diego, Calif.)*, *25*(4), 402–8. doi:10.1006/meth.2001.1262

Loevinger, R., Budinger, T. F., & Watson, E. E. (1991). *MIRD Primer For Absorbed Dose Calculations*. *The Society of Nuclear Medicine* (Revised Ed., p. 128). New York: The Society of Nuclear Medicine.

Maris, J. M., Hogarty, M. D., Bagatell, R., & Cohn, S. L. (2007). Neuroblastoma. *Lancet*, *369*(9579), 2106–20. doi:10.1016/S0140-6736(07)60983-0

Martin, J. E. (2006). *Physics for Radiation Protection: A Handbook* (2nd ed.). Weinheim: Wiley-VCH.

Martinez, A., Hinz, J. M., Gmez, L., Molina, B., Acua, H., Jones, I. M., … Coleman, M. a. (2008). Differential expression of TP53 associated genes in Fanconi anemia cells after mitomycin C and hydroxyurea treatment. *Mutation ResearchGenetic Toxicology and Environmental Mutagenesis*, *656*(1-2), 1–7. doi:10.1016/j.mrgentox.2008.06.012

Matthay, K. K., DeSantes, K., Hasegawa, B., Huberty, J., Hattner, R. S., Ablin, a, … Price, D. (1998). Phase I dose escalation of 131I-metaiodobenzylguanidine with autologous bone marrow support in refractory neuroblastoma. *Journal of Clinical Oncology : Official Journal of the American Society of Clinical Oncology*, *16*(1), 229–36. Retrieved from http://www.ncbi.nlm.nih.gov/pubmed/9440747

Matthay, K. K., Panina, C., Huberty, J., Price, D., Glidden, D. V, Tang, H. R., … Hasegawa, B. (2001). Correlation of tumor and whole-body dosimetry with tumor response and toxicity in refractory neuroblastoma treated with (131)I-MIBG. *Journal of Nuclear Medicine : Official Publication, Society of Nuclear Medicine*, *42*(11), 1713–21. Retrieved from http://www.ncbi.nlm.nih.gov/pubmed/11696644

Meredith, R. F., Wong, J. Y. C., & Knox, S. J. (2007). Targeted Radionuclide Therapy. In K. K. Ang, H. Choy, J. Harris, L. E. Kun, P. Mauch, E. G. Shaw, … A. L. Zietman (Eds.),

Clinical Radiation Oncology (2nd ed., pp. 407–436). Philadelphia: Elsevier Churchill Livingstone.

Monsieurs, M. A., Thierens, H. M., Vral, A., Brans, B., De Ridder, L., & Dierckx, R. A. (2001). Patient dosimetry after 131I-MIBG therapy for neuroblastoma and carcinoid tumours. *Nuclear Medicine Communications*, *22*(4), 367–374. doi:10.1097/00006231-200104000-00004

More, S., Itsara, M., Yang, X., & Geier, E. (2011). Vorinostat increases expression of functional norepinephrine transporter in neuroblastoma in vitro and in vivo model systems. *Clinical Cancer Research*, *17*, 2339–2349. doi:10.1158/1078-0432.CCR-10-2949

Morgan, W. F., & Bair, W. J. (2013). Issues in low dose radiation biology: the controversy continues. A perspective. *Radiation Research*, *179*(5), 501–10. doi:10.1667/RR3306.1

Munshi, A., Tanaka, T., Hobbs, M. L., Tucker, S. L., Richon, V. M., & Meyn, R. E. (2006). Vorinostat, a histone deacetylase inhibitor, enhances the response of human tumor cells to ionizing radiation through prolongation of gamma-H2AX foci. *Molecular Cancer Therapeutics*, *5*(8), 1967–74. doi:10.1158/1535-7163.MCT-06-0022

Paul, S., & Amundson, S. (2008). Development of gene expression signatures for practical radiation biodosimetry. *International Journal of Radiation Oncology* …*, *71*(4), 1236–1244. doi:10.1016/j.ijrobp.2008.03.043

Paul, S., Smilenov, L. B., & Amundson, S. a. (2013). Widespread decreased expression of immune function genes in human peripheral blood following radiation exposure. *Radiation Research*, *180*(6), 575–83. doi:10.1667/RR13343.1

Pecorino, L. (2008). *Molecular Biology of Cancer: Mechanisms, Targets, and Therapeutics* (2nd ed.). Oxford: Oxford University Press.

Pray, L. A. (2008). Eukaryotic Genome Complexity. *Nature Education*. Retrieved December 04, 2014, from http://www.nature.com/scitable/topicpage/eukaryotic-genome-complexity-437

R Core Team. (2013). R: A language and environment for statistical computing. Vienna, Austria: R Foundation for Statistical Computing.

Rana, S., Kumar, R., & Sharma, R. K. (2010). Radiation-induced biomarkers for the detection and assessment of absorbed radiation doses. *Journal of Pharmacy and Bioallied Sciences*, *2*(3), 189–196. Retrieved from http://www.ncbi.nlm.nih.gov/pmc/articles/PMC3148623/

Reed, E. (2010). DNA damage and repair in translational oncology: an overview. *Clinical Cancer Research*, *16*(18), 4511–4516. doi:10.1158/1078-0432.CCR-10-0528

Richon, V. M. (2006). Cancer biology : mechanism of antitumour action of vorinostat (suberoylanilide hydroxamic acid), a novel histone deacetylase inhibitor. *British Journal of Cancer*, *95*, S2–S6. doi:10.1038/sj.bjc.6603463

Riecke, a, Rufa, C., & Cordes, M. (2012). Gene expression comparisons performed for biodosimetry purposes on in vitro peripheral blood cellular subsets and irradiated individuals. *Radiation …*, *178*(3), 234–43. doi:10.1667/RR2738.1

Ropolo, M., Balia, C., Roggieri, P., Lodi, V., Nucci, M. C., Violante, F. S., … Bolognesi, C. (2012). The micronucleus assay as a biological dosimeter in hospital workers exposed to low doses of ionizing radiation. *Mutation Research*, *747*(1), 7–13. doi:10.1016/j.mrgentox.2012.02.014

Schaue, D., Kachikwu, E. L., & McBride, W. H. (2012). Cytokines in radiobiological responses: a review. *Radiation Research*, *178*(6), 505–23. doi:10.1667/RR3031.1

Snyder, A. R., & Morgan, W. F. (2004). Gene expression profiling after irradiation: clues to understanding acute and persistent responses? *Cancer Metastasis Reviews*, *23*(3-4), 259–68. doi:10.1023/B:CANC.0000031765.17886.fa

Snyder, W. S., Ford, M. R., Warner, G. G., & Watson, S. B. (1975). nm/mird Pamplet No. 11. *Society of Nuclear Medicine*. Retrieved June 04, 2014, from http://www.snmmi.org/files/docs/MIRD Pamphlet 11.174-257.pdf

Somasundaram, K., & El-Deiry, W. S. (2000). Tumor Suppressor P53: Regulation and Function. *Frontiers in Bioscience*, *5*(1), 424–437.

Sudbrock, F., Schmidt, M., Simon, T., Eschner, W., Berthold, F., & Schicha, H. (2010). Dosimetry for 131I-MIBG therapies in metastatic neuroblastoma, phaeochromocytoma and paraganglioma. *European Journal of Nuclear Medicine and Molecular Imaging*, *37*(7), 1279–90. doi:10.1007/s00259-010-1391-7

Swartz, H. M., Williams, B. B., & Flood, A. B. (2014). Overview of the principles and practice of biodosimetry. *Radiation and Environmental Biophysics*. doi:10.1007/s00411-014-0522-0

Tucker, J. D., Divine, G. W., Grever, W. E., Thomas, R. a, Joiner, M. C., Smolinski, J. M., & Auner, G. W. (2013). Gene expression-based dosimetry by dose and time in mice following acute radiation exposure. *PloS One*, *8*(12), e83390. doi:10.1371/journal.pone.0083390

Tucker, J. D., Joiner, M. C., Thomas, R. A., Grever, W. E., Bakhmutsky, M. V, Chinkhota, C. N., … Auner, G. W. (2014). Accurate gene expression-based biodosimetry using a minimal set of human gene transcripts. *International Journl of Radiation Oncology*, *88*(4), 933–939. Retrieved from http://www.ncbi.nlm.nih.gov/pubmed/24444760

Tucker, J. D., Vadapalli, M., Joiner, M. C., Ceppi, M., Fenech, M., & Bonassi, S. (2013). Estimating the lowest detectable dose of ionizing radiation by the cytokinesis-block micronucleus assay. *Radiation Research, 180*(3), 284–91. doi:10.1667/RR3346.1

Vassal, G., Giammarile, F., Brooks, M., Geoerger, B., Couanet, D., Michon, J., … Morland, B. (2008). A phase II study of irinotecan in children with relapsed or refractory neuroblastoma: A European cooperation of the Socie ´te ´ Franc ¸aise d'Oncologie Pe ´diatrique (SFOP) and the United Kingdom Children Cancer Study Group (UKCCSG). *European Journal of Cancer, 44*, 2453–2460. doi:10.1016/j.ejca.2008.08.003

Vöö, S., Bucerius, J., & Mottaghy, F. M. (2011). I-131-MIBG therapies. *Methods (San Diego, Calif.), 55*(3), 238–45. doi:10.1016/j.ymeth.2011.10.006

Wolden, S. (2007). Neuroblastoma. In K. K. Ang, H. Choy, J. Harris, L. E. Kun, P. Mauch, E. G. Shaw, … A. L. Zietman (Eds.), *Clinical Radiation Oncology* (2nd ed., pp. 1637–1643). Philadelphia: Elsevier Churchill Livingstone.

Wyrobek, A., & Manohar, C. (2011). Low dose radiation response curves, networks and pathways in human lymphoblastoid cells exposed from 1 to 10cGy of acute gamma radiation. *Mutation Reasearch, 722*(2), 119–130. doi:10.1016/j.mrgentox.2011.03.002

Zinkel, S., Gross, a, & Yang, E. (2006). BCL2 family in DNA damage and cell cycle control. *Cell Death and Differentiation, 13*(8), 1351–9. doi:10.1038/sj.cdd.4401987